Structural analysis of siloxane-containing calcium carbonate particles and tuning of their ion-releasing ability

シロキサン含有炭酸カルシウム粒子の構造解析と

そのイオン溶出制御に関する研究

Jin Nakamura

March 2014

Department of Frontier Materials

Nagoya Institute of Technology

Contents

Chapter I   Introduction

1   Contemporary clinical demands for bone defections and their treatments with biomaterials

The skeletal system in human has vital functions, namely mechanical, and structural support of the body, protection of organs, and reservoir of minerals for balances metabolisms.[1] Bone is a dynamic and vascularized, it enables to repair spontaneously without leaving a scar when it fractured.[2] However, sometimes these functions are disordered by trauma and pathologies.

Because of strong association with morbidity and mortality of elderly population, osteoporosis has been concerned as one of major socioeconomical and health-threatening issue in the today's aging society.[3] Imbalanced bone resorption by osteoclasts in the patients constructs a bone with lower mineral density with accumulated microfractures.[3-5] This raises the risk of bone fracture particularly at vertebra, femoral neck, hip and limb when a fatigue load is applied and increases the difficulties of daily activities.[3, 6-8] The demands for medical treatment and regenerative medicine in this pathology will keep growing up in the near future.

Periodontitis is also perilous to the regular living due to their direct effects to a daily dietary life. It is triggered by an infection at tooth roots.[9] Patients from adolescents to elderly populations has been reported and the symptoms known to be more progressive particularly in younger ages.[10] The progression of symptoms leads to the degeneration and loss of jaw bones, which causes the dislocation or unstable teeth. For the restoration of oral functions, even dental implantations and prior jaw reconstruction are required in the severe case with tooth exfoliations.[11]

Despite of spontaneous healing ability by homeostasis of bone tissues, the remodeling process results in the complex with nonunion or scars depending on the size of defections[12] and compromised metabolism by aging in some cases. In fact, yearly, 2.2 millions of population underwent orthopedic surgeries for the treatment of bone defects from trauma, congenital and resections subsequent to these diseases in worldwide.[13] The current golden standard in the clinical approaches is autologous bone grafts: fill a vacancy at defection with bone pieces which harvested from other body part such as iliac crests.[14, 15] Cells from host tissue, as well as cells in the graft facilitate new bone growth. However, there is a limitation in harvesting amounts of optimal bone pieces from donor sites. Besides, it imposes the morbidity with severe pains at the donor sites of the pieces on most of patients. To overcome this shortage, nonbiological materials have been used.

Calcium phosphates, in particular hydroxyapatite (HA) $(Ca_{10}(PO_4)_6(OH)_2)$ and β-tricalcium phosphate (β-TCP) $(Ca_3(PO_4)_2)$ are the most frequently used artificial bone grafts among the other ceramics-based biomaterials. HA has chemical similarity in composition to the native bones. This accounts for the integration of newly growing bone tissue without forming any fibrous tissue encapsulations.[16-18] β-TCP has advantages in resorbability by both simple dissolution and cellular

activities by osteoclasts, which are gradually replaced with native bones.[19, 20] These materials were commercially available in the various forms such as blocks, granules, porous. Due to the brittle nature, mostly these materials required to be used in mechanically stable conditions such as fixation with metal plates and screws.[21] Moreover, poor ability to actively induce osteogenesis comparing to autografts, which includes osteoblast cells from hosts, constrict their use to 10 % of total orthopedic procedures.[13]

The reconstruction procedure of jaw bone requires special concerns for intrude of soft tissues such as gums into the space of defections, which interrupt the bone ingrowth to induce failure with a nonunion. Guided bone regeneration (GBR) is a method which places barrier membranes between gums and the defections to allow spaces maintained to be filled with new bone.[22, 23] From the first successful procedure with polytetrafuluoroethylene (PTFE) membranes, this became the standard material in GBR membranes.[24] However, due to the requirement for secondary surgery to membrane removal, the use of biodegradable polymer membranes consisting of collagen, poly(lactic acid) (PLA) and poly(lactic-co-glycolic acids) (PLGA) were gradually increasing.[23, 25]

2   Genetical stimulation of bone turnover cycle by soluble silica species and calcium ion

A remodeling of living tissue requires transfer of a vast amount of information signal transduction among cells and organs. In the case of bone, osteoblasts and stem cells produce growth factors (GFs) such as transforming growth factor β (TGF-β), bone morphogenic proteins (BMPs), vascular endothelial growth factor (VEGF) and insulin-like growth factor (IGF). These GFs play an important role in regulating the cellular activities, such as stimulation or inhibition of cellular proliferation, differentiation, migration, adhesion, and gene expression, of cells at remodeling site.[26, 27]

Several works have looked at the incorporation of these GFs into biodegradable polymer-based scaffolds.[27-29] These materials were designed to promote the cellular activities by supplying the exogenous GFs as they degrade in the body. However, several issues exist, due to their short half-life (in the range of 1–4 h)[30] and the effective dose is severely dependent on the encapsulation and release rate from the scaffolds. Moreover, their exposure to organic solvents is known to cause denaturation of their protein structure.[31, 32] Besides, their high costs seize the use in general clinical opportunities.

In 1971, Hench et al. published a momentous report in which a glass of the composition 46.1 mol% SiO_2, 24.4 mol% Na_2O, 26.9 mol% CaO and 2.6 mol% P_2O_5, termed Bioglass[®] 45S5, formed a bond with native bone so strong that it could not pulled out without break the bone.[33] Later on they also reported the soluble silica species and calcium ions from Bioglass[®] 45S5 promote the bone

formation by stimulation of the genes within the osteoblast cells causing enhanced IGF-II expression.[34-37] The use of these inorganic ions as stimulation agent for bone formation is very promising and present the opportunity to reliably incorporate them in various scaffolds produced using methods that involve organic solvents and heating processes.[38, 39] Similarly silicon-doped hydroxyapatite (Actifuse, Baxter Pharmaceuticals, USA) has become the market leader for spinal fusion operations, which perform better than stoichiometric HA.[40, 41]

From the cell culture studies performed with the supplementation of calcium to the cell culture mediums, the fluctuation of extracellular calcium ion concentration ($[Ca^{2+}]_o$) has been known to regulate the metabolism cycles of osteogenic cells. The osteoclastic resorption of bone elevates local $[Ca^{2+}]_o$ to levels as high as 40 mM, which is reported to enhance the chemotaxis and proliferation of osteoblasts.[42-44] The proliferation or differentiation and mineralisation of osteoblasts were individually enhanced at specific levels of $[Ca^{2+}]_o$.[45-48] Nakade et al. reported the proliferation and differentiation of human osteoblasts were enhanced at 1.8-2.5 mM and the production of collagen type I, main organic component in bone, at approximatery 3mM.[45] Maeno et al. revealed that proliferation, differentiation/mineralization of mouse-derived osteoblasts were enhanced at 2-4 and 6-8 mM, respectively.[46] Therefore, controlling the calcium ion release from biomaterials is important to effectively encourage the vicinal bone reconstruction process.

3   Development of siloxane-containing vaterite (SiV) particles and their biomaterials

Calcium carbonates ($CaCO_3$) are one of the abundant mineral in nature, such as mollusk shells and corals. $CaCO_3$ has three anhydrous crystallographic polymorphs: thermodynamically least stable vaterite, aragonite, and the most stable calcite.

In 2002–2003, our fundamental reports of biomaterials containing vaterite were published. In which, composite pellet of PLA and about 1 μm-sized vaterite secondary particles, termed CCPC (calcium carbonate/poly(L-lactic acid) composites), were prepared.[49, 50] The vaterite enables immediate release of calcium ions upon soaking into a simulated body fluid (SBF): a physiological buffer solution which includes equivalent amount of minerals to human blood plasma. This calls the hydroxycarbonate apatite (HCA) layer formation on their surfaces within 1–3 days of soaking. This is important phenomena as their formation is the initial osteointegration event of biomaterials at host tissue.

Since the introduction of osteogenic stimulation ability is an important design for facilitate faster bone growth in the vicinity of biomaterials, second generation CCPCs with releasing ability of soluble silica were prepared by covalently bonding γ-aminopropyltriethoxysilane (APTES) to the carboxyl terminal of PLA matrices, termed Si-CCPC.[51] They were shaped into membranes for their aim to

use in GBR methods. According to soak in an SBF for 3 d, the HCA layers with including trace amount of Si were formed on their surfaces, which contributed to the improved proliferation of osteoblast cells, comparing to the membranes without the layers.

In order to achieve continuous releases of soluble silica species and calcium ions, besides to achieve versatility in use with variation of biodegradable polymers, particles of vaterite containing silsesquioxane (SiV) with a diameter of 1.5 μm were prepared via a carbonation process.[52, 53] This particle contains silsesquioxane derived from APTES. The aminopropyl groups provide organic functional sites to covalently bond with functional groups in polymers. At the implant site, the Si-O-Si bond in silsesquioxane hydrolyzes to produce soluble silica species. Besides, these particles were melt-blended with PLA to produce electrospun fibermats called SiPVH. The SiV particles were embedded in the PLA matrix.

The SiPVH electrospun fibermats were evaluated in vitro and in vivo.[52] When murine osteoblast-like cells (MC3T3-E1) were seeded, significantly larger numbers of the cells were observed on the SiPVH fibermats in comparison with that of a vaterite/PLA composite, which has no ability to release soluble silica species. The expression of ALP was also significantly higher on the SiPVH fibermats. Hence, the released ions from SiV were expected to successfully enhance the bone formation. The in vivo test was performed by covering a hole-shape defection (12 mmΦ) in rabbit calvaria with an SiPVH/PLA bilayered fibermat. After 4 w of culture, bone nodule was newly formed at the center area of the fibermat, where no host bone tissue was attached. These results demonstrated the high potential of the SiV particles and their biomaterials for the applications in bone regenerative medicines.

4   Aim of this thesis

The purpose of this thesis is to clarify the structure and reaction steps involved in the formation of SiV particles, and to expand the knowledge for controlling their ions releasing behavior, with the special emphasize of calcium ion through the structural nano-tune of vaterite. SiV particles offer much promise as materials for bone regeneration. We believe the biological properties of SiPVHs could be further enhanced through the optimization of their ion release. Previously the silsesquioxane and vaterite in the particles were individually characterized with ^{29}Si nuclear magnetic resonance spectrometry and X-ray diffractometry.[52] However, the mechanism of assembly and final structure of the SiV particles remained unclear. Understanding the structure of the particles influences their ion releasing behaviors.

In the current GBR procedures with the use of PLA or PLGA-based membranes, it is claimed to be necessary to use osteoconductive/osteoinductive fillers, due to their insufficient stiffness for maintaining the cavity of defections.[23] As a future application of SiV particles in the injectable

bone-fillling materials, composite microbeads of SiPVH were prepared by an electrospraying method.

In chapter II, the structure of SiV particles were discussed through the comparison of vaterite primary particles in SiV and stoichiometric vaterite. Their dissolution behaviors in physiological pH buffer solutions were also monitored, which provides an insight into the assemble ways of silsesquioxane and vaterite in an SiV particle. The precursor gel of SiV particles was characterized by means of time-resolved Fourier-transformed infrared spectrometry and laser Raman spectrometry to track the reactions involved in their formation from precursors.

In chapter III, the SiV particles consisting of orientated vaterite primary particles were prepared in the methanol-acetone mixed solvent. The (001) plane (*c*-face) of vaterite were known to possess high surface energy due to the exposure of Ca^{2+} or CO_3^{2-} uni-ionic plane.[54] The *c*/*ab*-face ratios of vaterite in SiV were attempted to control by varying the methanol:acetone volume fractions from 100:0 to 50:50; this hypothesized to influence the solubility of the vaterite primary particles. The ion releasing behaviors of these SiV particles were evaluated by soaking into a Tris buffer solution.

In chapter IV, in order to evaluate the possibility of drug loading, the SiV particles were prepared with using the equi-volume methanol-acetone mixed solvent in the presence/absence of low molecular weight PLA as a model drug. The structures of these particles were characterised by electron microscopy, a nitrogen adsorption analysis, X-ray diffractometry and spectroscopic analyses. The way of PLA loading in the particles is discussed. The dissolution tests of these particles were performed in the buffer solution.

Finally, chapter V describes the preparation of bead-shaped SiPVH with ion releasing ability for the application of minimal invasive cartilage reconstruction. The SiPVH beads with 10–60 wt% of SiV particles were prepared via the electrospraying method. To evaluate their degradation behavior, the beads were soaked in a Tris buffer solution. The slurry-feeding rate and the SiV content in the slurry were varied and their effect on bead diameter and morphology was investigated.

References

[1]   X. Wang, J. S. Nyman, X. Dong, H. Leng and M. Reyes, Fundamental biomechanics in bone tissue engineering. *Synthesis Lectures on Tissue Engineering*, **2**, 1-225 (2010).

[2]   D. Sommerfeldt and C. Rubin, Biology of bone and how it orchestrates the form and function of the skeleton. *Eur. Spine J.*, **10**, S86-S95 (2001).

[3]   S. Nojiri, R. T. Burge, J. A. Flynn, S. A. Foster and H. Sowa, Osteoporosis and treatments in japan: Management for preventing subsequent fractures. *J. Bone Miner. Metab.*, 1-14 (2013).

[4]   H. Orimo, Y. Sugioka, M. Fukunaga, Y. Muto, T. Hotokebuchi, I. Gorai, T. Nakamura, K. Kushida, H. Tanaka, T. Ikai and Y. Oh-hashi, Diagnostic criteria of primary osteoporosis. *J. Bone Miner. Metab.*, **16**, 139-150 (1998).

[5]   S. L. Teitelbaum, Osteoclasts, integrins, and osteoporosis. *J. Bone Miner. Metab.*, **18**, 344-349 (2000).

[6]   M. Takahashi, K. Kushida and K. Naitou, The degree of osteoporosis in patients with vertebral fracture and patients with hip fracture: Relationship to incidence of vertebral fracture. *J. Bone Miner. Metab.*, **17**, 187-194 (1999).

[7]   N. Yoshimura, T. Suzuki, T. Hosoi and H. Orimo, Epidemiology of hip fracture in japan: incidence and risk factors. *J. Bone Miner. Metab.*, **23**, 78-80 (2005).

[8]   H. Hagino, Features of limb fractures: A review of epidemiology from a japanese perspective. *J. Bone Miner. Metab.*, **25**, 261-265 (2007).

[9]   T. C. Hart and K. S. Kornman, Genetic factors in the pathogenesis of periodontitis. *Periodontol. 2000*, **14**, 202-215 (1997).

[10]   G. C. Armitage and M. P. Cullinan, Comparison of the clinical features of chronic and aggressive periodontitis. *Periodontol. 2000*, **53**, 12-27 (2010).

[11]   N. Sowmya and N. Kumar, Successful stabilization of periodontal disease and preprosthetic implant site preparation using autogenous mandibular symphysis block bone grafting in aggressive periodontitis. *J. Dent. Implant.*, **2**, 59 (2012).

[12]   H. Petite, V. Viateau, W. Bensaid, A. Meunier, C. de Pollak, M. Bourguignon, K. Oudina, L. Sedel and G. Guillemin, Tissue-engineered bone regeneration. *Nat. Biotechnol.*, **18**, 959-963 (2000).

[13]   K. U. Lewandrowski, J. D. Gresser, D. L. Wise and D. J. Trantolo, Bioresorbable bone graft substitutes of different osteoconductivities: A histologic evaluation of osteointegration of poly(propylene glycol-co-fumaric acid)-based cement implants in rats. *Biomaterials*, **21**, 757-764 (2000).

[14]   G. Zimmermann and A. Moghaddam, Allograft bone matrix versus synthetic bone graft substitutes. *Injury*, **42, Supplement 2**, S16-S21 (2011).

[15]   G. M. Calori, E. Mazza, M. Colombo and C. Ripamonti, The use of bone-graft substitutes in large bone defects: any specific needs? *Injury*, **42, Supplement 2**, S56-S63 (2011).

[16]   S. K. Ghosh, S. K. Nandi, B. Kundu, S. Datta, D. K. De, S. K. Roy and D. Basu, In vivo response of porous hydroxyapatite and β-tricalcium phosphate prepared by aqueous solution combustion method and comparison with bioglass scaffolds. *J. Biomed. Mater. Res., Part B*, **86B**, 217-227 (2008).

[17]   B. S. Chang, C. K. Lee, K. S. Hong, H. J. Youn, H. S. Ryu, S. S. Chung and K. W. Park, Osteoconduction at porous hydroxyapatite with various pore configurations. *Biomaterials*, **21**, 1291-1298 (2000).

[18]   U. Ripamonti, Osteoinduction in porous hydroxyapatite implanted in heterotopic sites of different animal models. *Biomaterials*, **17**, 31-35 (1996).

[19]   N. Kondo, A. Ogose, K. Tokunaga, T. Ito, K. Arai, N. Kudo, H. Inoue, H. Irie and N. Endo, Bone formation and resorption of highly purified β-tricalcium phosphate in the rat femoral condyle. *Biomaterials*, **26**, 5600-5608 (2005).

[20]   R. Fujita, A. Yokoyama, T. Kawasaki and T. Kohgo, Bone augmentation osteogenesis using hydroxyapatite and β-tricalcium phosphate blocks. *J. Oral Maxillofac. Surg.*, **61**, 1045-1053 (2003).

[21]   M. Bohner, L. Galea and N. Doebelin, Calcium phosphate bone graft substitutes: failures and hopes. *J. Eur. Ceram. Soc.*, **32**, 2663-2671 (2012).

[22]   C. H. F. Hämmerle and T. Karring, Guided bone regeneration at oral implant sites. *Periodontol. 2000*, **17**, 151-175 (1998).

[23]   M. Simion, A. Scarano, L. Gionso and A. Piattelli, Guided bone regeneration using resorbable and nonresorbable membranes: a comparative histologic study in humans. *Int. J. Oral Maxillofac. Implants*, **11**, 735-742 (1996).

[24]   J. M. Carbonell, I. S. Martín, A. Santos, A. Pujol, J. D. Sanz-Moliner and J. Nart, High-density polytetrafluoroethylene membranes in guided bone and tissue regeneration procedures: a literature review. *Int. J. Oral Maxillofac. Surg.*, DOI: 10.1016/j.ijom.2013.05.017 (2013).

[25]   G. Polimeni, K. T. Koo, G. A. Pringle, A. Agelan, F. F. Safadi and U. M. E. Wikesjö, Histopathological observations of a polylactic acid-based device intended for guided bone/tissue regeneration. *Clin. Implant. Dent. R.*, **10**, 99-105 (2008).

[26]   T. A. Linkhart, S. Mohan and D. J. Baylink, Growth factors for bone growth and repair: IGF, TGFβ and BMP. *Bone*, **19**, S1-S12 (1996).

[27]   P. Tayalia and D. J. Mooney, Controlled growth factor delivery for tissue engineering. *Adv. Mater.*, **21**, 3269-3285 (2009).

[28]   Z. Haidar, R. Hamdy and M. Tabrizian, Delivery of recombinant bone morphogenetic proteins for bone regeneration and repair. Part B: Delivery systems for BMPs in orthopaedic and craniofacial tissue engineering. *Biotechnol. Lett.*, **31**, 1825-1835 (2009).

[29]   J. H. Lee, H. W. Jung, I. K. Kang and H. B. Lee, Cell behaviour on polymer surfaces with different functional groups. *Biomaterials*, **15**, 705-711 (1994).

[30]   K. Takaoka, M. Koezuka and H. Nakahara, Telopeptide-depleted bovine skin collagen as a carrier for bone morphogenetic protein. *J. Orthop. Res.*, **9**, 902-907 (1991).

[31]   G. Crotts and T. G. Park, Protein delivery from poly(lactic-co-glycolic acid) biodegradable microspheres: release kinetics and stability issues. *J. Microencapsul.*, **15**, 699-713 (1998).

[32]   K. Fu, K. Griebenow, L. Hsieh, A. M. Klibanov and L. Robert, FTIR characterization of the secondary structure of proteins encapsulated within PLGA microspheres. *J. Controlled Release*, **58**, 357-366 (1999).

[33]   L. L. Hench, The story of Bioglass®. *J. Mater. Sci. Mater. Med.*, **17**, 967-978 (2006).

[34]   I. D. Xynos, A. J. Edgar, L. D. K. Buttery, L. L. Hench and J. M. Polak, Ionic products of bioactive glass dissolution increase proliferation of human osteoblasts and induce insulin-like growth factor II mRNA expression and protein synthesis. *Biochem. Biophys. Res. Commun.*, **276**, 461-465 (2000).

[35]   I. D. Xynos, A. J. Edgar, L. D. K. Buttery, L. L. Hench and J. M. Polak, Gene-expression profiling of human osteoblasts following treatment with the ionic products of Bioglass® 45S5 dissolution. *J. Biomed. Mater. Res.*, **55**, 151-157 (2001).

[36]   I. D. Xynos, M. V. J. Hukkanen, J. J. Batten, L. D. Buttery, L. L. Hench and J. M. Polak, Bioglass®45S5 stimulates osteoblast turnover and enhances bone formation; implications and applications for bone tissue engineering. *Calcif. Tissue Int.*, **67**, 321-329 (2000).

[37]   J. E. Gough, J. R. Jones and L. L. Hench, Nodule formation and mineralisation of human primary osteoblasts cultured on a porous bioactive glass scaffold. *Biomaterials*, **25**, 2039-2046 (2004).

[38]   A. R. Boccaccini, M. Erol, W. J. Stark, D. Mohn, Z. Hong and J. F. Mano, Polymer/bioactive glass nanocomposites for biomedical applications: a review. *Composites Sci. Technol.*, **70**, 1764-1776 (2010).

[39]   A. Hoppe, N. S. Güldal and A. R. Boccaccini, A review of the biological response to ionic dissolution products from bioactive glasses and glass-ceramics. *Biomaterials*, **32**, 2757-2774 (2011).

[40]   N. Patel, S. M. Best, W. Bonfield, I. R. Gibson, K. A. Hing, E. Damien and P. A. Revell, A comparative study on the in vivo behavior of hydroxyapatite and silicon substituted hydroxyapatite granules. *J. Mater. Sci. Mater. Med.*, **13**, 1199-1206 (2002).

[41]   E. S. Thian, J. Huang, M. E. Vickers, S. M. Best, Z. H. Barber and W. Bonfield, Silicon-substituted hydroxyapatite (SiHA): A novel calcium phosphate coating for biomedical applications. *J. Mater. Sci.*, **41**, 709-717 (2006).

[42]   T. Sugimoto, M. Kanatani, J. Kano, H. Kaji, T. Tsukamoto, T. Yamaguchi, M. Fukase and K. Chihara, Effects of high calcium concentration on the functions and interactions of osteoblastic cells and monocytes and on the formation of osteoclast-like cells. *J. Bone Miner. Res.*, **8**, 1445-1452 (1993).

[43]   S. L. Godwin and S. P. Soltoff, Extracellular calcium and platelet-derived growth factor promote receptor-mediated chemotaxis in osteoblasts through different signaling pathways. *J. Biol. Chem.*, **272**, 11307-11312 (1997).

[44]   T. Yamaguchi, N. Chattopadhyay, O. Kifor, R. R. Butters, T. Sugimoto and E. M. Brown, Mouse osteoblastic cell line (MC3T3-E1) expresses extracellular calcium (Ca^{2+}_o)–sensing receptor and its agonists stimulate chemotaxis and proliferation of MC3T3-E1 cells. *J. Bone Miner. Res.*, **13**, 1530-1538 (1998).

[45]   O. Nakade, K. Takahashi, T. Takuma, T. Aoki and T. Kaku, Effect of extracellular calcium on the gene expression of bone morphogenetic protein-2 and -4 of normal human bone cells. *J. Bone Miner. Metab.*, **19**, 13-19 (2001).

[46]   S. Maeno, Y. Niki, H. Matsumoto, H. Morioka, T. Yatabe, A. Funayama, Y. Toyama, T. Taguchi and J. Tanaka, The effect of calcium ion concentration on osteoblast viability, proliferation and differentiation in monolayer and 3D culture. *Biomaterials*, **26**, 4847-4855 (2005).

[47]   M. M. Dvorak, A. Siddiqua, D. T. Ward, D. H. Carter, S. L. Dallas, E. F. Nemeth and D. Riccardi, Physiological changes in extracellular calcium concentration directly control osteoblast function in the absence of calciotropic hormones. *Proc. Natl. Acad. Sci. U. S. A.*, **101**, 5140-5145 (2004).

[48]   E. Eklou-Kalonji, I. Denis, M. Lieberherr and A. Pointillart, Effects of extracellular calcium on the proliferation and differentiation of porcine osteoblasts in vitro. *Cell Tissue Res.*, **292**, 163-171 (1998).

[49]   H. Maeda, T. Kasuga, M. Nogami, Y. Hibino, K. I. Hata, M. Ueda and Y. Ota, Biomimetic apatite formation on poly (lactic acid) composites containing calcium carbonates. *J. Mater. Res.*, **17**, 727-730 (2002).

[50]   T. Kasuga, H. Maeda, K. Kato, M. Nogami, K.-i. Hata and M. Ueda, Preparation of poly(lactic acid) composites containing calcium carbonate (vaterite). *Biomaterials*, **24**, 3247-3253 (2003).

[51]   H. Maeda, T. Kasuga and L. L. Hench, Preparation of poly(l-lactic acid)-polysiloxane-calcium carbonate hybrid membranes for guided bone regeneration. *Biomaterials*, **27**, 1216-1222 (2006).

[52]   A. Obata, T. Hotta, T. Wakita, Y. Ota and T. Kasuga, Electrospun microfiber meshes of silicon-doped vaterite/poly(lactic acid) hybrid for guided bone regeneration. *Acta Biomater.*, **6**, 1248-1257 (2010).

[53]   T. Wakita, J. Nakamura, Y. Ota, A. Obata, T. Kasuga and S. Ban, Effect of preparation route on the degradation behavior and ion releasability of siloxane-poly(lactic acid)-vaterite hybrid nonwoven fabrics for guided bone regeneration. *Dent. Mater. J.*, **30**, 232-238 (2011).

[54]   N. Gehrke, H. Cölfen, N. Pinna, M. Antonietti and N. Nassif, Superstructures of calcium carbonate crystals by oriented attachment. *Cryst. Growth Des.*, **5**, 1317-1319 (2005).

Chapter II   Tracking the formation of vaterite particles containing aminopropyl-functionalized silsesquioxane and their structure for bone regenerative medicine

1   Introduction

Remodeling of living tissue involves a large amount of signal transduction among cells and organs. In the case of bone, osteoblast and stem cells produce growth factors (GFs) such as transforming growth factor β (TGF-β), bone morphogenic proteins, vascular endothelial growth factor (VEGF) and insulin-like growth factor (IGF). These GFs play an important role in regulating the proliferation and differentiation of cells at remodeling site.

Several works have looked at the incorporation of these GFs into biodegradable organic scaffolds.[1-3] These materials were designed to promote the cellular activities by supplying the exogenous GFs as they degrade in the body. However, several issues exist, due to their short half-life (in the range of 1 - 4 h)[4] and the effective dose is severely dependent on the encapsulation and release rate from the scaffolds. Moreover, their exposure to organic solvents is known to cause denaturation of their protein structure.[5, 6] Thus, the encapsulation processes of the GFs must be carefully selected. Another strategy that has been exploited to promote the proliferation and differentiation of cells towards osteoblasts is to provide dissolution products such as soluble silica and calcium ions.

Hench group reported the soluble silica species and calcium ions from Bioglass® 45S5 promote the bone formation by stimulation of the genes within the osteoblast cells causing enhanced IGF-II expression.[7-9] The use of these inorganic ions as stimulation agent for bone formation is very promising and present the opportunity to reliably incorporate them in various scaffolds produced using methods that involve organic solvents and heating processes.[10, 11] Similarly silicon-doped hydroxyapatite (Actifuse, Baxter Pharmaceuticals, USA) has become the market leader for spinal fusion operations, which perform better than stoichiometric HA[12, 13], even though there are also critical opinions, which point to the passive effect of Si-substitution such as alteration of calcium release from the material, changes in surface chemistry and topography.[14]

Previously, the authors developed particles of vaterite containing silsesquioxane (SiV) with a diameter of 1 μm for use with poly(lactic acid) (PLA) to produce electrospun fibermats called SiPVH.[15, 16] The SiV particles were embedded in the PLA matrix. Vaterite is the least thermodynamically stable polymorph of calcium carbonate, so on contact with body fluid they immediately dissolved, supplying calcium ions, while a part of them re-crystalize as the most stable calcite. Simultaneously carbonate ions are also released, which contribute to neutralize the pH decrease at the inflamed implantation site. The SiV particles also contain silsesquioxane derived from γ-aminopropyltriethoxysilane (APTES). The aminopropyl groups provide organic functional sites to

covalently bond with carboxyl groups in PLA. At the implant site, the Si–O–Si bond in silsesquioxane hydrolyzes to produce soluble silica species. The SiPVH electrospun fibermats were evaluated *in vitro* and *in vivo*.[15] When murine osteoblast-like cells (MC3T3-E1) were seeded, significantly larger numbers of the cells were observed on the SiPVH fibermats in comparison with that of a vaterite/PLA composite, which has no ability to release soluble silica species. The expression of ALP was also significantly higher on the SiPVH fibermats. Hence, the released ions from SiV were expected to successfully enhance the bone formation. The *in vivo* test was performed by covering a hole-shape defect (12 mmΦ) in rabbit calvaria with an SiPVH/PLA bilayered fibermat. After 4 w of culture, bone nodule was newly formed at the center area of the fibermat, where no host bone tissue was attached.

Gough *et al.* reported that specific amounts of soluble silica and calcium ions were required to promote cell activity therefore its vital to control the release rate.[9] SiV particles offer much promise as materials for bone regeneration. Previously the silsesquioxane and vaterite in the particles were individually characterized with ^{29}Si nuclear magnetic resonance spectrometry and X-ray diffractometry.[15] However, the mechanism of assembly and final structure of the SiV particles remained unclear. The present work aims to explore the mechanism of formation of the SiV and to understand its physical structure and chemical properties. The structure of the particles possibly affects their ion releasing behavior. In order to achieve an insight into the effect, dissolution of SiV particles in physiological pH was also performed.

2 Experimental Section

2.1 Synthesis and Characterization of SiV particles

SiV particles were synthesized by following the carbonation method in methanol described elsewhere.[15] 100 ml of distilled water, 150 g of calcium hydroxide (Wako Pure Chemicals Inc., Japan, Medical grade), 60 or 150 ml of γ-aminopropyltriethoxysilane (Momentive Performance Materials Inc., Japan, denoted as APTES) were added in order to 2 L of methanol (Wako Pure Chemicals Inc., Japan, Medical grade) while stirring. Each reagent was added at 20 min intervals. Carbon dioxide gas was introduced to the slurry with a rate of 2 L min^{-1} for 60 min, resulting in a translucent precursor gel. The gel was aged for 12 h at room temperature then heated at 110 °C for 24 h to remove residual solvents. During the aging process gel samples were collected every 1 h and analyzed by attenuated total reflectance Fourier transform infrared spectroscopy (JASCO, FTIR 4000 spectrometer equipped with ATR PRO 450-S attachment : ATR-FTIR spectroscope) and laser Raman spectroscopy (JASCO, NRS-2000 : LR spectroscope) with argon-ion laser operated at 514.5 nm. The resulting powder was then ground to result in the SiV particles. The silicon contents of the SiV particles were estimated by X-ray fluorescence spectrometry (XRF). Vaterite particles with no Si addition were also synthesized by the carbonation process. This will be referred to as V.

X-ray diffraction (XRD) and ATR-FTIR techniques were used to study the crystal and chemical structure of the particles. The morphologies of particles were observed with a scanning electron microscope (SEM) using an accelerating voltage of 15kV (JEOL, JSM-6301F). The mean diameters of particles were estimated from the SEM images using ImageJ software (http://rsbweb.nih.gov/ij/, n=10).

To image the cross section of V and $Si_{2.6}V$ particles they were embedded in epoxy resin, then sections were prepared by focused gallium ion beam (FIB) milling (FEI, Helios NanoLab 600 dual beam FIB). The samples were observed with TEM at 200 kV (JEOL, JEOL-2010) equipped with an energy-dispersive X-ray spectrometer (EDX, Oxford Instruments, X-Max 80 mm^2 EDX detector with INCA software).

2.2   Dissolution of SiV particles

Tris buffer was prepared in a water bath warmed at 36.5 °C, where 6.118 g of tris(hydroxymethyl)aminomethane was dissolved in 900 ml of distilled water. The pH was adjusted to 7.40 using 1.0 M hydrochloric acid solution. The resulting solution was transfered to a 1 L volumetric flask, and brought to the volume with distilled water to achieve 0.05 M Tris buffer solution.

In polystyrene containers, 0.5 g of $Si_{2.6}V$, $Si_{4.9}V$ and vaterite particles were immersed in 20 ml of the Tris buffer solution and incubated at 36.5 °C. After 1, 3, 6, 12 and 24 h of soaking period, the samples were filtered and dried at 50 °C.

The dried samples were evaluated with an X-ray diffractometer (PANalytical, X'pert-MPD : XRD) and the ATR-FTIR. The concentrations of soluble silica and calcium ion in the soaking solutions were measured with an inductively coupled plasma atomic emission spectrometer (Shimadzu, ICPS-7000 : ICP-AES). (n=3)

The $Si_{2.6}V$ particles were also soaked in a Mili-Q water (ion-exchanged ultra pure water prepared with Millipore Milli-Q Synthesis purification system) to eliminate the undesirable effect from the solvent. The sample to solution ratio was adjusted to 10 g / 10 ml. After 48 h of soaking, the sample was centrifuged at 5,000 rpm for 5 min. The supernatant solution was then filtered with a PTFE syringe filter (pore size : 0.2 μm). ^{29}Si nuclear magnetic resonance (^{29}Si NMR) spectrum of the resulting solution was recorded on a Varian UNITY Inova 400 plus NMR spectrometer operating at 79.49 MHz.

3 Results and discussion

3.1 Characteristics of the SiV particles

SiV particles were prepared by a carbonation process supplementing with 60 and 150 ml of APTES. The resulting particles were estimated to contain 2.6 and 4.9 wt% of silicon by XRF spectrometry, respectively. Hereafter, the SiV are denoted as Si_xV where x is the silicon content in the particles (x = 2.6, 4.9). Figure 2–1(a, b, c) shows the SEM images of V, $Si_{2.6}V$ and $Si_{4.9}V$ particles, respectively. The V particles were spherical with the mean diameter of 0.7 μm (standard deviation, SD=0.1). $Si_{2.6}V$ particles had spherical morphology with the mean diameter of 1.4 μm (SD=0.1). The surface texture of these particles was smoother compared to that of the V particles. $Si_{4.9}V$ particles had the mean diameter of 1.5 μm (SD=0.1). An aggregation of smaller particles was observed on their surfaces, which gave irregular texture to the particles.

TEM images of V particle cross-sections show uniform rounded primary particles densely aggregated to form the spherical secondary particles (Fig. 2–2(a)). The primary particles had a mean diameter of approximately 65 nm (n=20, SD=7, Fig. 2–2(b)). Fig. 2–2(c) shows that the polycrystalline electron diffraction pattern obtained on the V sample was that of vaterite with the d spacing and (hkl) values of 2.21 Å (116), 1.85 Å (304), 1.34 Å (412), and 1.15 Å (334) (JCPDS No. 33-0268). Since the $Si_{2.6}V$ and $Si_{4.9}V$ have identical components, they were assumed to possess similar nanostructures. Therefore, $Si_{2.6}V$ particles were chosen for the TEM observation. According to the sectional image of $Si_{2.6}V$ particle, defined primary particle structure could not be observed (Fig. 2–2(d) and Fig. 2–2(e)). The sample mostly provided amorphous electron diffraction patterns with undefined Debye rings (results are not shown). The TEM images show a gradient in atomic contrast along the cross-section of the particle, where a calcium-rich center appeared darker while the edge, which had a lower concentration of calcium was brighter. This suggests that calcium carbonate (vaterite) particles were relatively concentrated in the core of the particles. An EDX mapping image and a line scan profile in Fig. 2–2(f) of a single $Si_{2.6}V$ particle shows this more clearly. It shows that the calcium atom count was significantly more intense in the center of the particle. Moreover, Si/Ca atom count ratio showed higher value in the edge of particle comparing to the central part. These results suggested that the calcium carbonate in $Si_{2.6}V$ was enclosed by a region, which was relatively rich in silicon. From the high magnification images, lamellae of vaterite with the length of 5-20 nm were observed as dark contrast part (Fig 2–2(e)): these were significantly smaller than the primary particles of V particle.

These samples were further characterized with XRD (Fig. 2–3). Both samples showed diffraction patterns of vaterite with the $P6_3/mmc$ space group (JCPDS No. 33-0268). The peaks at $21°$ and $25°$ originated from diffraction of (004) and (110) planes of their hexagonal unit cell, which are the representative of c and ab faces of the hexagonal unit lattice. The peak integrated area ratios ($I_{(004)}$ /

$I_{(110)}$) of V and $Si_{2.6}V$ were 0.14 and 0.22, respectively. This suggesting that the vaterite in $Si_{2.6}V$ particles was slightly orientated to c face. Generally, the crystalline face of vaterite is known to be highly polarized due to the exposure of the Ca^{2+} or CO_3^{2-} uni-ionic planes and stabilized by the coordination of counter ionic species.[17, 18] In the $Si_{2.6}V$, silsesquioxane (from APTES) presumably contributes to the stabilization of the c-face.

Figure 4 shows the ATR-FTIR spectra of V and SiV particles. In the spectrum of V particles, absorption bands were observed at 1409, 1087, 875 and 745 cm^{-1}. These bands originate from asymmetric stretch (v_3), symmetric stretch (v_1), out of plane bending (v_2) and in-plane bending (v_4) of carbonate, respectively. Particularly, the emergence of v_1 and v_4 bands at the given wavenumbers represents the carbonate ion from crystalline vaterite.[19, 20] The bands were also observed in the spectra from $Si_{2.6}V$ and $Si_{4.9}V$. Both SiV particles showed notably broadened v_3 bands in the region around 1400 cm^{-1} compared to V particles. Besides, the broadening was slightly greater in the spectrum from $Si_{4.9}V$. Due to lack in the symmetry of the carbonate ion position, spectra of amorphous calcium carbonate (ACC) have splitting of v_3 bands at 1420 and 1474 cm^{-1}.[19-21] The band broadening in SiV suggests the presence of ACC. The ACC is reported to form in the presence of various chemical species, such as inorganic ions (e.g. magnesium ion[20], triphosphate ion[22]), macromolecules rich in carboxylic group (e.g. poly(acrylic acid)[23], poly(aspartic acid)[24]) and phosphonates.[25] These species are considered to adsorb on the surface of nascent calcium carbonate nuclei and physically suppress or interrupt the transportation of ions, leading to the transient stabilization of amorphous phase. In the case of SiV particles, silsesquioxane derived from APTES could play the role of these stabilizers.

FTIR spectra from $Si_{2.6}V$ and $Si_{4.9}V$ particles contained bands at 1125 cm^{-1}, which was assigned to the asymmetric stretch of Si–O–Si bonds from APTES-derived silsesquioxane. The Si–O–Si bonds form by condensation of Si–OH groups, created by the hydrolysis of the APTES. A small band in 925 cm^{-1} was assigned to the stretching mode of Si–O bond from non-bridging silanol groups (Fig. 4. inset). The Si–O bond indicates that there were uncondensed Si–OH bonds in the APTES. ^{29}Si magic angle spinning nuclear magnetic resonance spectrometry (MAS-NMR) of $Si_{2.6}V$ particles was performed in our previous work.[15] The notation T^n species (n = 0~3) indicate the connectivity of the trialkoxysilanes, with a T^3 species representing a silicon atom bonded to three other silicon atoms through bridging Si–O–Si bonds, while T^0 species represent a silicon atom with three non-bridging oxygens (NBOs). The silsesquioxanes in SiV were found to consist of only T^2 and T^3 species; no T^0 and T^1 species were observed. T^0 and T^1 would imply unreacted APTES was present. The abundance of T^2 and T^3 were approximately 30 and 70%, respectively. Thus, the observed Si–O group was originated from NBO in the T^2 species. Zhmud et al. reported fundamental research on the structure of APTES-modified silica.[26, 27] According to the report, the silanol non-bridging group on the surface of silica is deprotonated in a stable manner in polar media by the intermolecular proton transfer to

aminopropyl groups, to form Si–O$^-$...H$_3$N$^+$ structure. Silanol groups are well reported to adsorb cations through ion exchange.[28-30] Silanol groups are also known to be effective for biomimetic apatite nucleation as Ca^{2+} ion and other cations attracting center.[31, 32] During the SiV synthesis, the negatively charged silanol groups of reacting APTES might interact with calcium ion. This may take a role in the stabilization of vaterite and ACC.
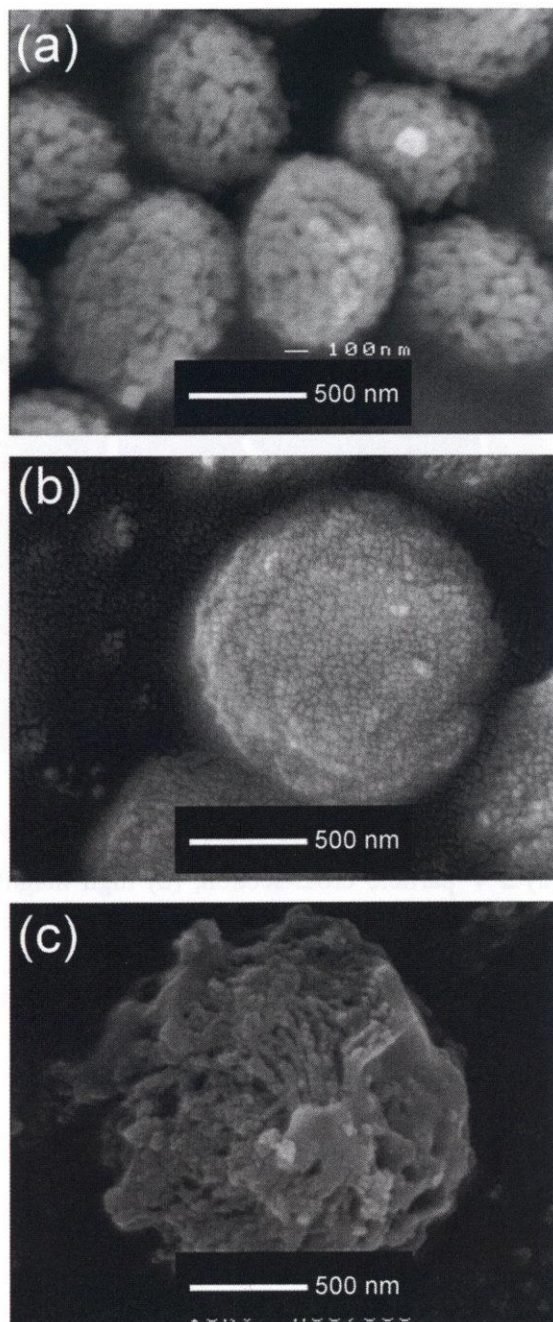
Fig. 2–1. SEM images of (a) V, (b) $Si_{2.6}V$ and (c) $Si_{4.9}V$ particles.
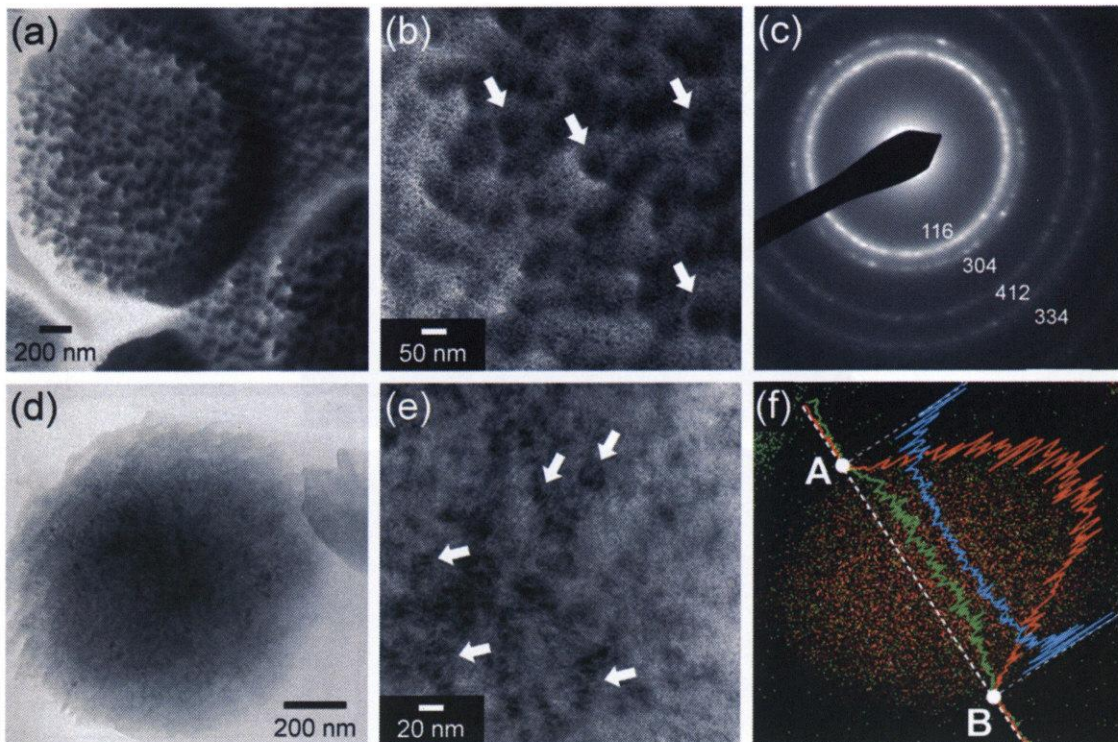
Fig. 2–2. TEM images of (a) a V particle cross-section, (b) high magnification image of (a), (c) electron diffraction pattern of V primary particles, (d) a $Si_{2.6}V$ particle cross-section, (e) highly magnified image of central part of (d), (f) EDX atomic map of single $Si_{2.6}V$ particle with line scan profile of A-B (green : Si, red : Ca, blue : atom count ratio of Si/Ca). Arrows in (b, e) indicate typical primary particles of vaterite.
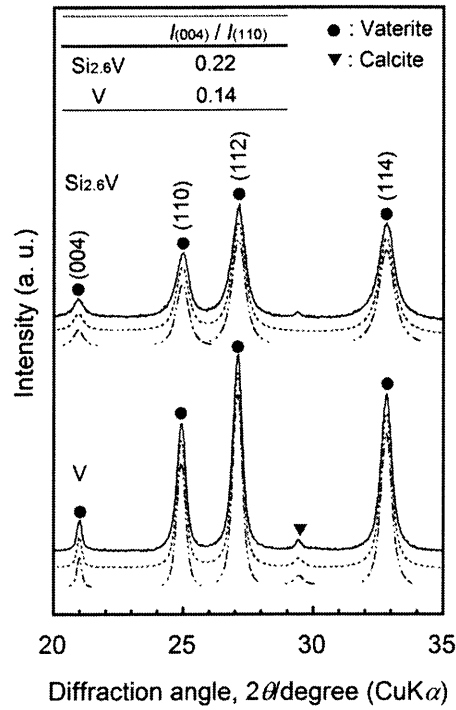
Fig. 2–3. XRD patterns of V and $Si_{2.6}V$ particles. Break lines indicate the Voigt function-fitted individual peaks and whole patterns. Inset table shows the peak integrated area ratios of diffraction peaks from (004) and (110).
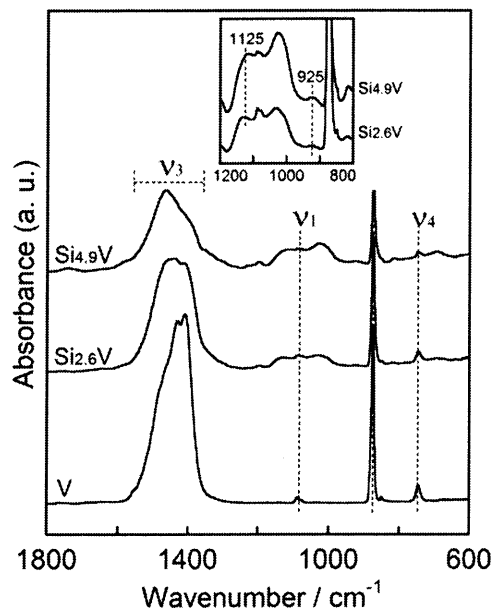
Fig. 2–4. ATR-FTIR spectra of V, $Si_{2.6}V$ and $Si_{4.9}V$ particles. The inset shows the high intensified spectra of the SiV particles.

3.2   Reactions in the aging process of SiV particles

For the evaluation of SiV formation, the precursor gel of $Si_{2.6}V$ was analyzed with ATR-FTIR and LR spectrometers during the aging process. Figure 2–5(a) shows the ATR-FTIR spectra of $Si_{2.6}V$ precursor gel at 0~7 h of aging. After CO_2 blowing and before the aging process (0 h), small broad band was observed at 859 cm^{-1} and was assigned to the v_2 of carbonate ions in ACC. After 1~2 h of aging, a shoulder band formed at 876 cm^{-1}. This is assigned to the v_2 of crystalline calcium carbonate, the crystallization of ACC started at about this time point. The ratio of absorbance (876)/absorbance (859) increased with aging time. After 5~7 h of aging, v_4 of vaterite was observed at around 740 cm^{-1}.

LR spectra of the precursor gels at 0~5 h are shown in Fig. 2–5(b). At the beginning of aging, peaks at 654 and 610 cm^{-1} were observed: These are the typical peaks from the vibration of R-Si(OR')$_3$ (R' = H, C_2H_5) structure in unhydrolysed or uncondensed APTES molecules.[33, 34] Most of the R' groups were thought to be hydrogen since the peak of C–C–O structure from ethanol were observed at 879 cm^{-1}, which is produced by the hydrolysis of ethoxy groups in an APTES molecule. The condensation of the APTES was confirmed after 1 h aging from the peak of Si–O–Si bonding at 515 cm^{-1}. The peak intensities of the R–Si(OR')$_3$ species decreased as aging time increased and completely disappeared after 5 h, where the most of the silanol groups from the hydrolyzed APTES were assumed to have condensed.

According to the FT–IR and LR spectrometries, SiV particles may form during the aging process with the reaction steps as follows (Fig. 2–6). At the beginning of aging (0 h), the precursor gel contains nascent nuclei of ACC, Ca^{2+} ions, protonated carbonate ions and uncondensed APTES molecules. During 1 to 7 h of aging, competing reaction of siloxane and vaterite formations take place. the maturation of ACC gradually proceeds to from the vaterite lamellae. Simultaneously Si–OH groups in hydrolysed APTES molecules condence to form silsesquioxane in the vicinity of the vaterite and ACC. They contains negatively charged silanol groups, which may adsorb to the Ca^{2+} ion plane of the calcium carbonates, which leading to the stabilization of the premature crystalline phases. The silsesquioxane grows to enclose calcium carbonate particles and aggregate each other. After 12 h of the process, their aggregation proceeds and they precipitate as a 1.4 μm-sized spherical SiV particle.
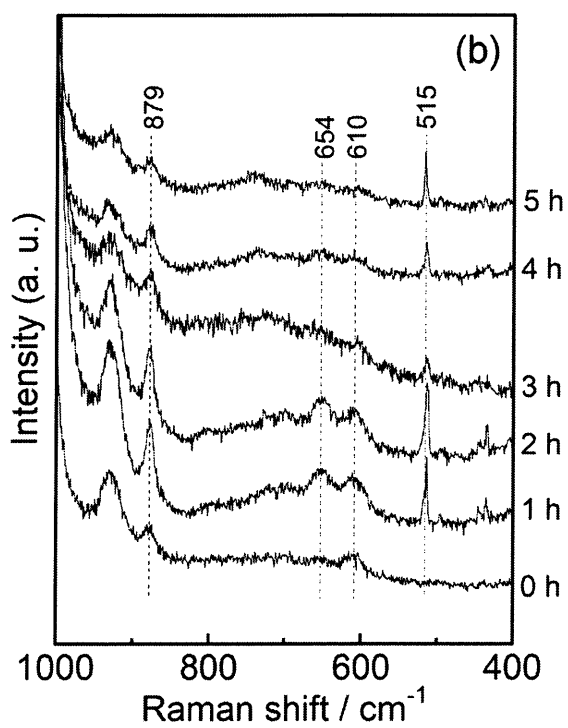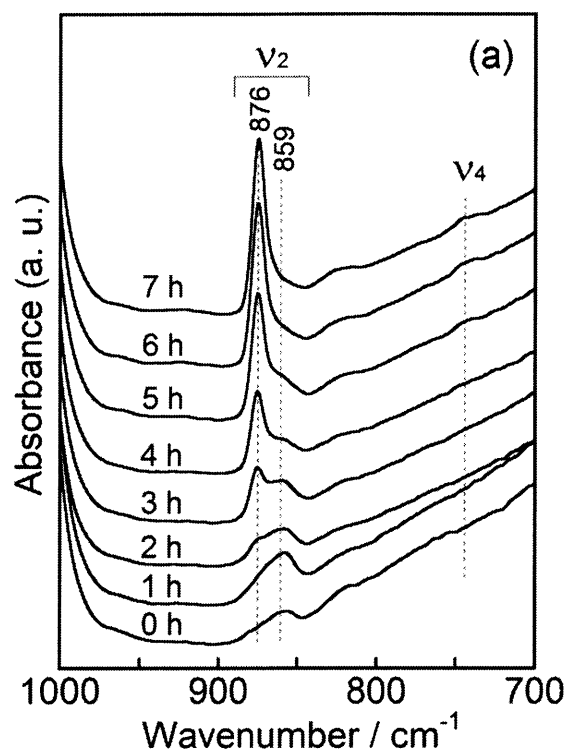
Fig. 2–5. ATR–FTIR spectra (a) and LR spectra (b) of an $Si_{2.6}V$ precursor gel after the given periods of aging process.
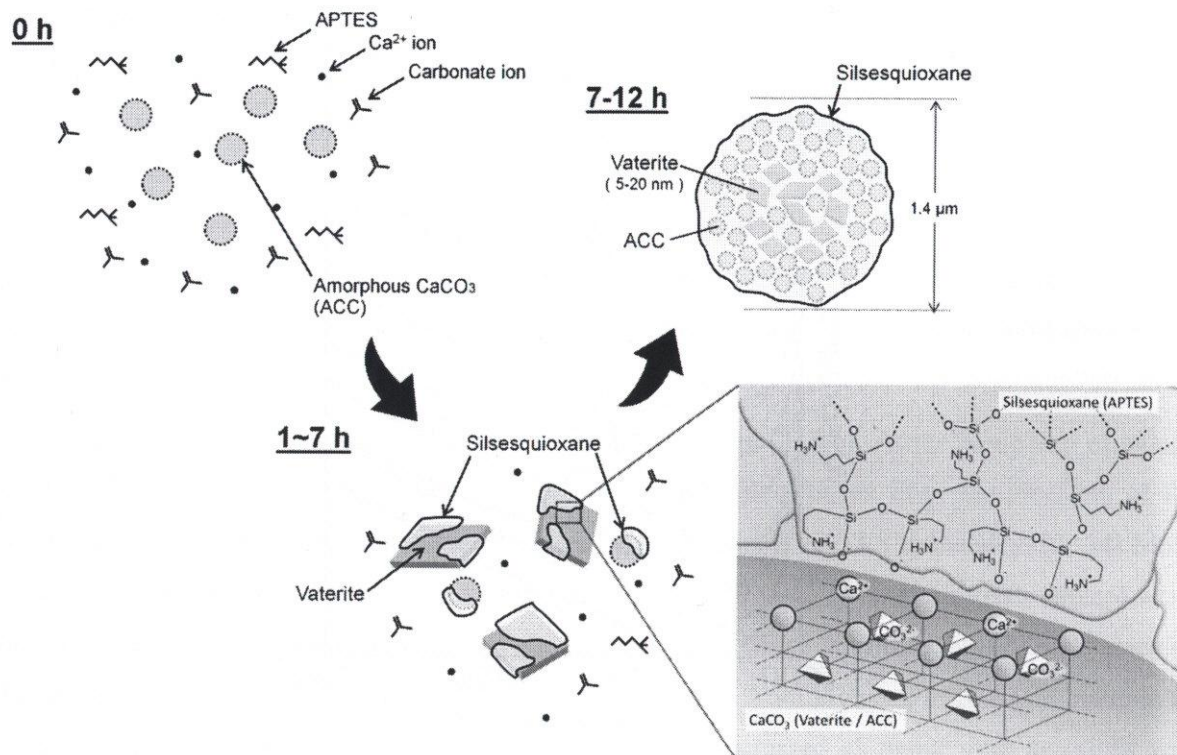
Fig. 2-6. Prospected formation steps involved in the formation of an SiV particle. At the beginning of aging, the precursor gel includes nascent nuclei of amorphous calcium carbonate (ACC), calcium ions, carbonate ions and APTES molecules. During 1-7 h of aging, the ACC crystallizes to vaterite. Simultaneously, the APTES molecules condense in the vicinity of the vaterite. Silanol groups in the APTES adsorb to the ACC and growing vaterite. After 7 h of aging, APTES derived silsesquioxane enclose vaterite and ACC, as well as aggregate with other primary particles to form an SiV particle.

3.3 Dissolution behavior of SiV particles

Dissolution of the SiV particles was investigated by soaking in Tris buffer solution. Figure 2–7 shows the XRD pattern of the SiV particles after soaking in Tris buffer solution for 0, 1, 3, 6, 12 and 24 h. In the $Si_{2.6}V$ particles, the peaks for vaterite were present before soaking. After 1 h of soaking, a peak around 29°, which is the main peak of calcite, appeared. After 3 h, the intensity of vaterite peaks decreased as peaks for calcite increased and after 6 h of soaking the vaterite peaks totally disappeared. This vaterite-calcite transformation took place more slowly in the $Si_{4.9}V$ particles. The vaterite peaks remained distinguishable after 12 h of soaking. In contrast, when the V particles containing no Si were soaked in Tris buffer solution, all vaterite peaks disappeared after just 1 h of soaking (indicated in fig. 2–12). Generally, vaterite is a metastable-crystalline phase thus, in a highly humidified environment they immediately convert into calcite, which is the most stable calcium carbonate through a dissolution/reprecipitation process. This implies that the vaterite in an SiV particle is transiently stabilized by the coexisting components.

Figure 2–8 shows the ATR-FTIR spectra of SiV particles at given soaking time points. In the spectra from $Si_{2.6}V$ particles, the absorption band at 1125 cm^{-1} assigned to Si–O–Si bonding decreased after 1 h. The band totally disappeared after 3 h of soaking, which suggests the release of majority of the silsesquioxane from SiV particles. At the same time, the v_3 band of carbonate ions narrowed and shifted towards 1409 cm^{-1} after 1 h of soaking. This indicates the release of ACC from $Si_{2.6}V$ particles. In the spectra from $Si_{4.9}V$ particles, the decrease in v_3 band width and absorption at 1125 cm^{-1} were observed after 1 h. This indicates the release of silsesquioxane and ACC during the initial period of soaking. Particularly, the band at 1125 cm^{-1} was present after 6 h of soaking. Therefore, part of the silsesquioxane still remained in the $Si_{4.9}V$ particles.

Based on the dissolution behaviors, vaterite in the SiV particles is suggested to be enclosed by APTES-derived silsesquioxane and ACC, which is in good agreement with the structure observed in TEM-EDX analysis. Once in contact with Tris buffer solution, the silsesquioxane and the ACC layers are released, while the vaterite core is physically stabilized until majority of the outer shell is released. The SiV particles with higher silicon content released the silsesquioxane with increasing periods of soaking, which was found to significantly influence the stabilization time of vaterite.

Figure 2–9 shows the soluble silica and Ca^{2+} ion concentrations in the Tris buffer solution after soaking $Si_{2.6}V$ and $Si_{4.9}V$ particles for given time points. Large increases in the concentration of the dissolution products were observed from both SiV particles within the initial hour of soaking. This trend originates from the release of the silsesquioxane and ACC in the SiV particles. After 3 h of soaking, the soluble silica concentration leached 21 mmol L^{-1}, corresponding to the 90 % of total silsesquioxane content in $Si_{2.6}V$ particles. Total release of silsesquioxane from the $Si_{2.6}V$ and $Si_{4.9}V$ particles were confirmed after 6 h and 24 h, respectively. The concentration of Ca^{2+} ion decreased at 3 h in both SiV particles, after which no significant changes were observed. According to the XRD,

calcite is formed in the soaked sample. Thus, the dissolution and precipitation of calcite are considered to achieve equilibrium in the Tris buffer solution.

Since the soluble silica species from SiV were produced by the hydrolysis of silsesquioxane, their structures are likely to vary. ^{29}Si NMR spectrometry of leached products from $Si_{2.6}V$ into Mili-Q water provided insights into their structures.

According to the ^{29}Si NMR spectrum (Fig. 2–10), peaks were observed at –42, –51, –59 and –68 ppm, which are assigned to the T^0, T^1, T^2 and T^3 species, respectively.[35, 36] The T^0 species represents the existence of monomeric-aminopropylsilanetriols. This species is reported to have a zwitterion-like structure in aqueous solutions[37] as depicted in Fig. 2–11(a). The T^1 species may originate from their dimers (Fig. 2–11(b)). The T^2 and T^3 species suggests the existence of comparably larger sized structures, such as oligomers. The oligomeric trialkoxysilanes are known to form polyhedral silica networks; each vertex is occupied by silicon atoms.[38-40] Detailed discussion on their sizes is difficult without employing a size exclusion chromatography and a mass spectrometry analyses. The T^2 and T^3 species, however presumably form structures as depicted in Fig. 2–11(c); the aminopropylsilanetriols form incomplete polyhedral structure with silanol groups. Besides, the amino groups are protonated considering the pKa of propylamines.[41]

The relative abundance of these T species were estimated from their Gaussian fitting curves of the ^{29}Si NMR spectra; approximately 10, 25, 45 and 20 % were occupied by T^0, T^1, T^2 and T^3 species, respectively. Considering the structure of silsesquioxane in SiV; consist of T^2 and T^3 species[15], the result indicated that on contact with moisture, Si–O–Si bonding in the silsesquioxane are hydrolyzed to produce the oligomers. Consequently some oligomers undergo further hydrolysis to produce the monomers and dimers in the soaking solutions.
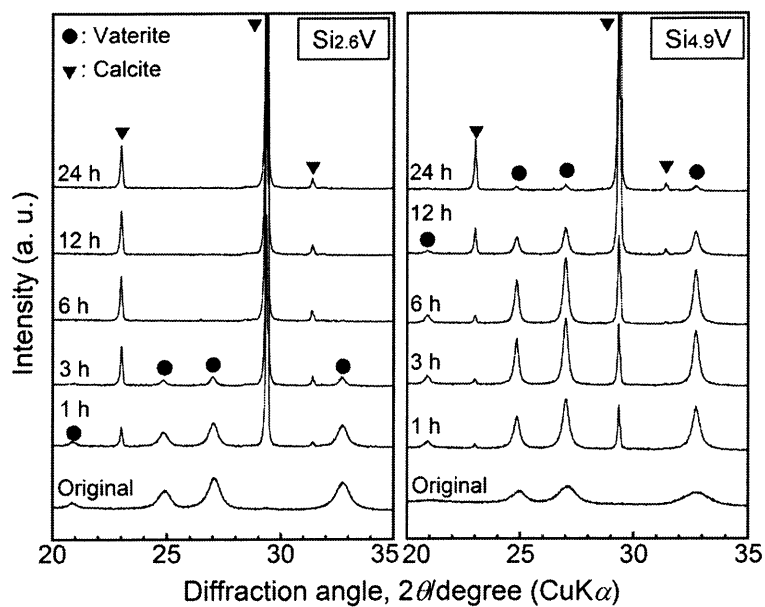
Fig. 2–7. XRD patterns of $Si_{2.6}V$ and $Si_{4.9}V$ particles after being soaked in Tris buffer solution after given soaking time.
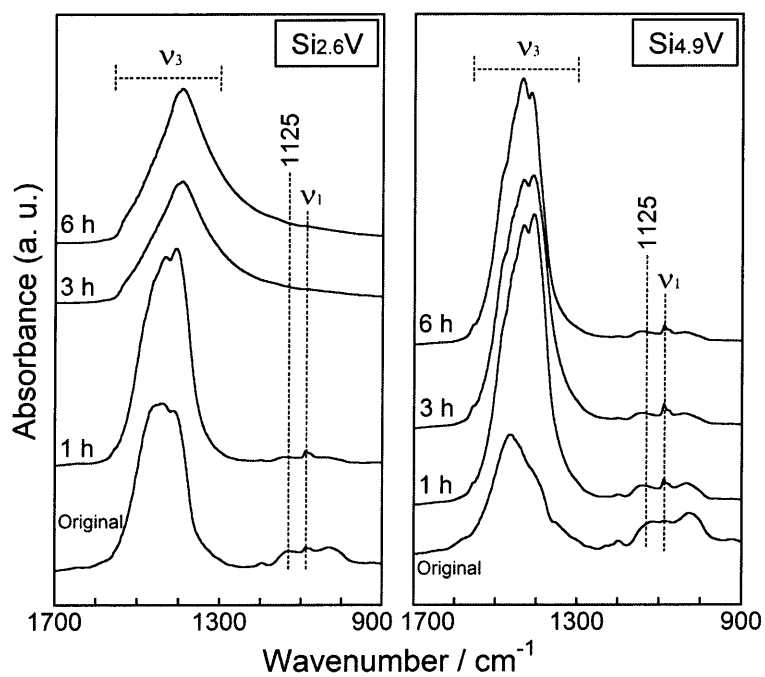
Fig. 2–8. ATR-FTIR spectra of $Si_{2.6}V$ and $Si_{4.9}V$ particles after being soaked in Tris buffer solution after given time.

25
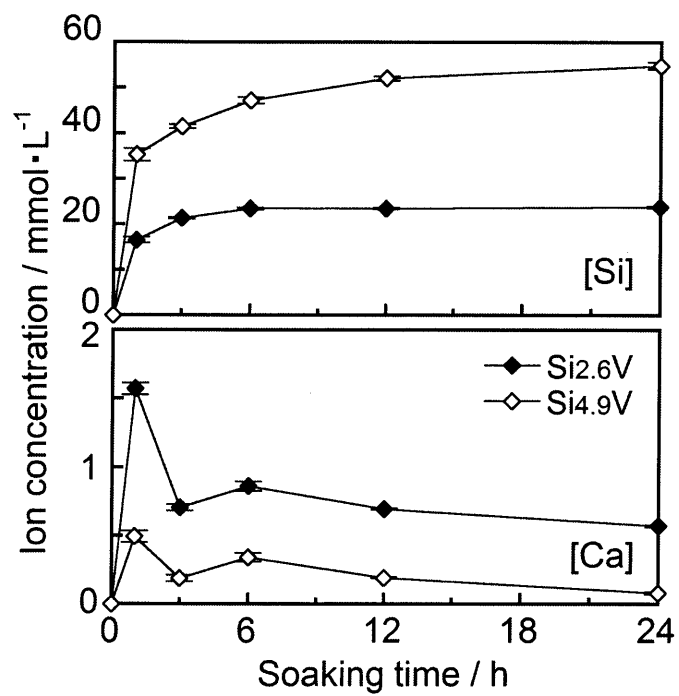
Fig. 2–9. Soluble silica and Ca^{2+} ions concentrations in Tris buffer solutions after soaking $Si_{2.6}V$ and $Si_{4.9}V$ particles for given soaking time.
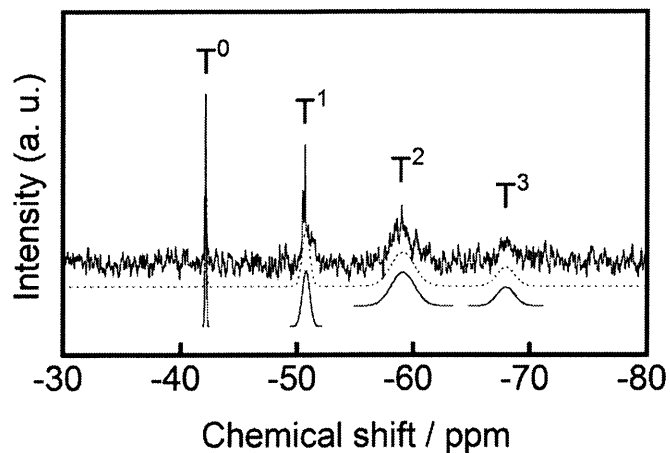
Fig. 2-10. ^{29}Si NMR spectrum of Mili-Q water after soaking $Si_{2.6}V$ particles for 48 h. Dotted- and continuous lines indicate Gaussian fitting curves of total spectrum and individual peaks, respectively.
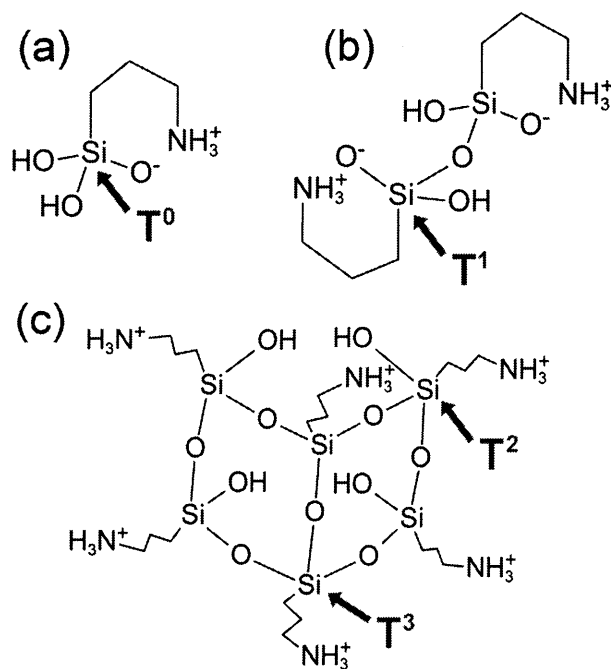
Fig. 2-11. Prospected structures of soluble silica species being released from $Si_{2.6}V$ particles. (a) monomeric-, (b) dimeric- and (c) oligomeric species.
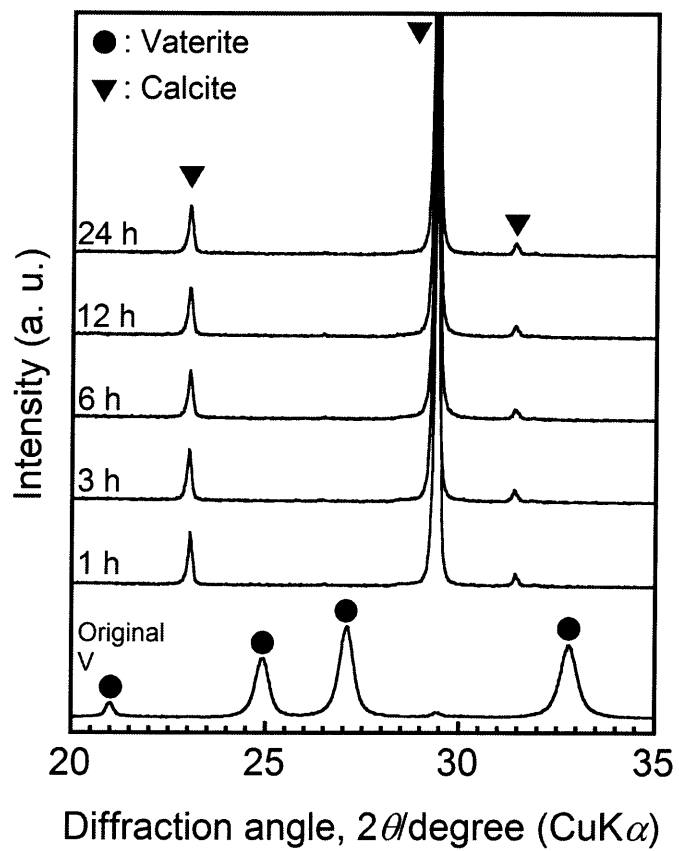
Fig.2–12. XRD patterns of V particles after being soaked in Tris buffer solution after given time.

4 Conclusions

- SiV particles were synthesized by a carbonation process in the presence of APTES.

- The 5–20 nm sized vaterite lamellae in $Si_{2.6}V$ were enclosed in APTES-derived silsesquioxane and amorphous calcium carbonate.

- During the aging of precursor gel, the condensation of the silsesquioxane and the crystallization of the vaterite were found to begin within initial an 1~2 h of aging and proceed concurrently up to 7 h of analysis period.

- In the Tris buffer solution, silsesquioxane and ACC promptly dissolved from the particles. Vaterite gradually dissolve and transformed into calcite along with the dissolution of silsesquioxane.

- The total dissolution times of the silsesquioxane were 6 h and 24 h for $Si_{2.6}V$ and $Si_{4.9}V$ particles, which was found to significantly influence the transformation time of vaterite.

- When the particles were also soaked in Mili-Q water, the T^2 species of silicon atoms were predominantly found in their leached product, which is followed by the T^1 and T^3 species.

References

[1]   Z. Haidar, R. Hamdy and M. Tabrizian, Delivery of recombinant bone morphogenetic proteins for bone regeneration and repair. Part B: delivery systems for bmps in orthopaedic and craniofacial tissue engineering. *Biotechnol. Lett.*, **31**, 1825-1835 (2009).

[2]   P. Tayalia and D. J. Mooney, Controlled growth factor delivery for tissue engineering. *Adv. Mater.*, **21**, 3269-3285 (2009).

[3]   K. Lee, E. A. Silva and D. J. Mooney, Growth factor delivery-based tissue engineering: general approaches and a review of recent developments. *J. R. Soc. Interface*, **8**, 153-170 (2011).

[4]   K. Takaoka, M. Koezuka and H. Nakahara, Telopeptide-depleted bovine skin collagen as a carrier for bone morphogenetic protein. *J. Orthop. Res.*, **9**, 902-907 (1991).

[5]   G. Crotts and T. G. Park, Protein delivery from poly(lactic-co-glycolic acid) biodegradable microspheres: release kinetics and stability issues. *J. Microencapsul.*, **15**, 699-713 (1998).

[6]   K. Fu, K. Griebenow, L. Hsieh, A. M. Klibanov and L. Robert, FTIR characterization of the secondary structure of proteins encapsulated within PLGA microspheres. *J. Controlled Release*, **58**, 357-366 (1999).

[7]   I. D. Xynos, M. V. J. Hukkanen, J. J. Batten, L. D. Buttery, L. L. Hench and J. M. Polak, Bioglass$^®$45S5 stimulates osteoblast turnover and enhances bone formation; implications and applications for bone tissue engineering. *Calcif. Tissue Int.*, **67**, 321-329 (2000).

[8]   I. D. Xynos, A. J. Edgar, L. D. K. Buttery, L. L. Hench and J. M. Polak, Gene-expression profiling of human osteoblasts following treatment with the ionic products of bioglass$^®$ 45S5 dissolution. *J. Biomed. Mater. Res.*, **55**, 151-157 (2001).

[9]   J. E. Gough, J. R. Jones and L. L. Hench, Nodule formation and mineralisation of human primary osteoblasts cultured on a porous bioactive glass scaffold. *Biomaterials*, **25**, 2039-2046 (2004).

[10]   A. R. Boccaccini, M. Erol, W. J. Stark, D. Mohn, Z. Hong and J. F. Mano, Polymer/bioactive glass nanocomposites for biomedical applications: a review. *Composites Sci. Technol.*, **70**, 1764-1776 (2010).

[11]   A. Hoppe, N. S. Güldal and A. R. Boccaccini, A review of the biological response to ionic dissolution products from bioactive glasses and glass-ceramics. *Biomaterials*, **32**, 2757-2774 (2011).

[12]   N. Patel, S. M. Best, W. Bonfield, I. R. Gibson, K. A. Hing, E. Damien and P. A. Revell, A comparative study on the in vivo behavior of hydroxyapatite and silicon substituted hydroxyapatite granules. *J. Mater. Sci. Mater. Med.*, **13**, 1199-1206 (2002).

[13]   E. S. Thian, J. Huang, M. E. Vickers, S. M. Best, Z. H. Barber and W. Bonfield, Silicon-substituted hydroxyapatite (SiHA): a novel calcium phosphate coating for biomedical applications. *J. Mater. Sci.*, **41**, 709-717 (2006).

[14]   M. Bohner, Silicon-substituted calcium phosphates – a critical view. *Biomaterials*, **30**, 6403-6406 (2009).

[15]   A. Obata, T. Hotta, T. Wakita, Y. Ota and T. Kasuga, Electrospun microfiber meshes of silicon-doped vaterite/poly(lactic acid) hybrid for guided bone regeneration. *Acta Biomater.*, **6**, 1248-1257 (2010).

[16]   T. Wakita, J. Nakamura, Y. Ota, A. Obata, T. Kasuga and S. Ban, Effect of preparation route on the degradation behavior and ion releasability of siloxane-poly(lactic acid)-vaterite hybrid nonwoven fabrics for guided bone regeneration. *Dent. Mater. J.*, **30**, 232-238 (2011).

[17]   N. Gehrke, H. Cölfen, N. Pinna, M. Antonietti and N. Nassif, Superstructures of calcium carbonate crystals by oriented attachment. *Cryst. Growth Des.*, **5**, 1317-1319 (2005).

[18]   A. W. Xu, M. Antonietti, H. Cölfen and Y. P. Fang, Uniform hexagonal plates of vaterite $CaCO_3$ mesocrystals formed by biomimetic mineralization. *Adv. Funct. Mater.*, **16**, 903-908 (2006).

[19]   L. Addadi, S. Raz and S. Weiner, Taking advantage of disorder: Amorphous calcium carbonate and its roles in biomineralization. *Adv. Mater.*, **15**, 959-970 (2003).

[20]   E. Loste, R. M. Wilson, R. Seshadri and F. C. Meldrum, The role of magnesium in stabilising amorphous calcium carbonate and controlling calcite morphologies. *J. Cryst. Growth*, **254**, 206-218 (2003).

[21]   P. K. Ajikumar, L. G. Wong, G. Subramanyam, R. Lakshminarayanan and S. Valiyaveettil, Synthesis and characterization of monodispersed spheres of amorphous calcium carbonate and calcite spherules. *Cryst. Growth Des.*, **5**, 1129-1134 (2005).

[22]   J. R. Clarkson, T. J. Price and C. J. Adams, Role of metastable phases in the spontaneous precipitation of calcium carbonate. *J. Chem. Soc., Faraday Trans.*, **88**, 243-249 (1992).

[23]   S. C. Huang, K. Naka and Y. Chujo, Effect of molecular weights of poly(acrylic acid) on crystallization of calcium carbonate by the delayed addition method. *Polym. J*, **40**, 154-162 (2007).

[24]   J. Aizenberg, G. Lambert, S. Weiner and L. Addadi, Factors involved in the formation of amorphous and crystalline calcium carbonate: a study of an ascidian skeleton. *J. Am. Chem. Soc.*, **124**, 32-39 (2001).

[25]   K. Sawada, The mechanisms of crystallization and transformation of calcium carbonates. *Pure Appl. Chem.*, **69**, 8 (1997).

[26]   B. V. Zhmud and J. Sonnefeld, Aminopolysiloxane gels: production and properties. *J. Non-Cryst. Solids*, **195**, 16-27 (1996).

[27] A. A. Golub, A. I. Zubenko and B. V. Zhmud, γ-APTES modified silica gels: The structure of the surface layer. *J. Colloid Interface Sci.*, **179**, 482-487 (1996).

[28] S. M. Ahmed and A. B. Van Cleave, Adsorption and flotation studies with quartz: part I. adsorption of calcium, hydrogen and hydroxyl ions on quartz. *Can. J. Chem. Eng.*, **43**, 23-26 (1965).

[29] A. J. Dent, J. D. F. Ramsay and S. W. Swanton, An EXAFS study of uranyl ion in solution and sorbed onto silica and montmorillonite clay colloids. *J. Colloid Interface Sci.*, **150**, 45-60 (1992).

[30] S. K. Milonjić, A relation between the amounts of sorbed alkali cations and the stability of colloidal silica. *Colloids Surf.*, **63**, 113-119 (1992).

[31] P. Li, C. Ohtsuki, T. Kokubo, K. Nakanishi, N. Soga, T. Nakamura and T. Yamamuro, Apatite formation induced by silica gel in a simulated body fluid. *J. Am. Ceram. Soc.*, **75**, 2094-2097 (1992).

[32] S. B. Cho, K. Nakanishi, T. Kokubo, N. Soga, C. Ohtsuki, T. Nakamura, T. Kitsugi and T. Yamamuro, Dependence of apatite formation on silica gel on its structure: effect of heat treatment. *J. Am. Ceram. Soc.*, **78**, 1769-1774 (1995).

[33] P. T. K. Shih and J. L. Koenig, Raman studies of the hydrolysis of silane coupling agents. *Mater. Sci. Eng.*, **20**, 137-143 (1975).

[34] B. Riegel, S. Blittersdorf, W. Kiefer, S. Hofacker, M. Müller and G. Schottner, Kinetic investigations of hydrolysis and condensation of the glycidoxypropyltrimethoxysilane/aminopropyltriethoxy-silane system by means of FT-Raman spectroscopy I. *J. Non-Cryst. Solids*, **226**, 76-84 (1998).

[35] I. Shimizu, H. Okabayashi, N. Hattori, K. Taga, A. Yoshino and C. O'Connor, ^{13}C- and ^{1}H-NMR and FTIR spectroscopic evidence for aggregate formation of organosilanes in toluene. *Colloid. Polym. Sci.*, **275**, 293-297 (1997).

[36] Y. Sugahara, S. Okada, S. Sato, K. Kuroda and C. Kato, ^{29}Si-NMR study of hydrolysis and initial polycondensation processes of organoalkoxysilanes. II. methyltriethoxysilane. *J. Non-Cryst. Solids*, **167**, 21-28 (1994).

[37] H. Ishida, C. H. Chiang and J. L. Koenig, The structure of aminofunctional silane coupling agents: 1. γ-aminopropyltriethoxysilane and its analogues. *Polymer*, **23**, 251-257 (1982).

[38] J. F. Brown, L. H. Vogt and P. I. Prescott, Preparation and characterization of the lower equilibrated phenylsilsesquioxanes. *J. Am. Chem. Soc.*, **86**, 1120-1125 (1964).

[39] C. L. Frye and W. T. Collins, Oligomeric silsesquioxanes, $(HSiO_{3/2})_n$. *J. Am. Chem. Soc.*, **92**, 5586-5588 (1970).

[40] J. D. Miller, K. P. Hoh and H. Ishida, Studies of the simulation of silane coupling agent structures on particulate fillers; the pH effect. *Polym. Compos.*, **5**, 18-28 (1984).

[41]   M. Guillot, M. Richard-Plouet and S. Vilminot, Structural characterisations of a lamellar organic-inorganic nickel silicate obtained by hydrothermal synthesis from nickel acetate and (aminopropyl)triethoxysilane. *J. Mater. Chem.*, **12**, 851-857 (2002).

Chapter III   Enhancement of crystalline plane orientation in silsesquioxane-containing vaterite particles towards tuning of calcium ion release

1   Introduction

In the remodelling process of bone, osteoblasts and stem cells produce growth factors (GFs) such as insulin-like growth factor-II (IGF-II), bone morphogenetic proteins (BMP) and transforming growth factor β (TGFβ). These GFs act as signal transducers among cells and tissues and regulates their proliferation and differentiation at the remodelling site.[1, 2]

A trace amount of soluble silica species and calcium ions from Bioglass® 45S5 has been reported to stimulate genes within the osteoblast cells to enhance IGF-II expression, thereby causing promoted bone formation.[3-5] The use of these inorganic ions as an osteogenic promoter presents the opportunity to reliably incorporate them into various biomaterials for bone reconstruction surgery. Similarly silicon-doped hydroxyapatite (Actifuse®, Baxter Pharmaceuticals, USA), which perform better than stoichiometric HA, has been used extensively in spinal fusion operations.[6, 7]

We previously developed a method for the preparation of silsesquioxane-containing vaterite (SiV) spherical particles with a diameter of 1.5 μm via a carbonation process.[8-10] Vaterite is the least thermo-dynamically stable polymorph among calcium carbonates. In the SiV particles, vaterite is included as 5–20 nm-sized lamellae. They are enclosed and transiently stabilised using silsesquioxane derived from γ-aminopropyltriethoxysilane (APTES).[11] Upon contact with a physiological pH buffer solution, the Si–O–Si bond in the silsesquioxane hydrolyses to release soluble silica species. This release triggers the subsequent release of calcium ions from vaterite. In addition, simultaneously, carbonate ions, which help counteract the decrease in pH at the inflamed implantation site, are released.

The SiV particles were incorporated into poly(lactic acid) (PLA) electrospun fibermats and evaluated *in vitro* and *in vivo*.[8, 9] When murine osteoblast-like cells are seeded, significantly enhanced proliferation and alkaline phosphatase (ALP) expression, which is a marker of calcification, are observed on the fibermats in comparison to a pure vaterite/PLA fibermat. Hence, the leached products from SiV are expected to enhance bone formation. We performed the *in vivo* test by covering a hole-shaped defect in rabbit calvaria with an SiV/PLA fibermat. After 4 w, bone nodules were newly formed at the middle part of the fibermat, where no native bone was contacted.

The fluctuation of extracellular calcium ion concentration ($[Ca^{2+}]_o$) is known to regulate the bone metabolism cycle by influencing osteogenic cellular activities. The osteoclastic resorption of bone elevates local $[Ca^{2+}]_o$ to levels as high as 40 mM, which is known to enhance the chemotaxis and proliferation of osteoblasts.[12-14] The proliferation or differentiation and mineralisation of murine osteoblast were individually enhanced at specific levels of $[Ca^{2+}]_o$.[15-17] Therefore, controlling the

calcium ion release from biomaterials is important to effectively encourage the vicinal bone reconstruction process. With respect to SiV particles, tailoring the solubility of primary vaterite particles is vital for achieving their controlled release. During the preparation of calcium carbonates, the degree of supersaturation influences the kinetics of formation, such as the rate of formation or size and morphology of particles. Acetone is a conventional aprotic solvent that has lower electrophilicity compared with methanol.[18, 19] When these solvents are mixed in certain volume fractions, their electrophilicity decreases in a controlled manner, which increases the supersaturation of carbonate ion to influence the crystallisation rate of vaterite.

In this work, we demonstrate a simple method for controlling the superstructure of SiV particles and the c-face orientation of internal primary vaterite particles through the use of a methanol–acetone mixed solvent in the carbonation process. The dissolution/ion release behaviours of the resulting SiV particles were then investigated in a physiological pH buffer solution to evaluate the influence of the c-face orientation on the particles' calcium ion release.

2   Materials and methods

2.1   Preparation of SiV particles

SiV particles were prepared by a carbonation method in methanol or methanol–acetone mixed solvents. In brief, 15 ml of distilled water, 22.5 g of calcium hydroxide (Yabashi Industries Co., Ltd., Japan) and 8.5 g of γ-aminopropyltrimethoxysilane (APS; Sigma-Aldrich Japan, Tokyo, Japan) were added into 300 ml of absolute methanol or methanol–acetone mixed solvent (methanol:acetone = 70:30 or 50:50 vol. ratio) (Wako Pure Chemicals Inc., Japan) under stirring. Carbon dioxide gas was introduced into the slurry at a rate of 2 L min^{-1} for 60 min, which resulted in the formation of a translucent precursor gel. The gel was aged for 12 h at room temperature and then heated at 110 °C for 1 day to remove residual solvents. The resulting powders were then ground, which resulted in the formation of SiV particles.

The silicon contents of the samples were estimated by X-ray fluorescence spectrometry (XRF). Hereafter, the SiV particles are referred to as SiV-xM(100 − x)A, where x is the volume% of methanol in the preparation solvent (x = 100, 70, 50). X-ray diffraction (XRD; PANalytical, X'pert-MPD) and ^{29}Si magic angle spinning nuclear magnetic resonance spectrometry (^{29}Si MAS-NMR; Varian, UNITY Inova 400 plus NMR spectrometer, operated at 79.49 MHz) were used to study the chemical structure of the silsesquioxane.

The morphologies of the particles were observed by scanning electron microscopy (SEM; JEOL, JSM-6301F, operated at 5 kV). To image the cross-section of SiV-50M50A particles, they were embedded in epoxy resin, and sections were subsequently prepared by focused gallium ion beam

milling (JEOL, EM-9320FIB). The samples were observed by transmission electron microscopy (TEM; JEOL, JEM-2010HR) on an instrument operated at 200 kV.

2.2   Dissolution test in Tris buffer solution

For the dissolution study, Tris buffer solution was prepared in a water bath warmed to 36.5 °C, where 6.118 g of tris(hydroxymethyl)aminomethane (Wako Pure Chemicals Inc., Japan) was dissolved in 900 ml of distilled water. The pH value was adjusted to 7.40 using 1.0 M hydrochloric acid solution (Wako Pure Chemicals Inc., Japan). The resulting solution was transferred to a 1-L volumetric flask, and the volume was brought to 1 L with distilled water to achieve a 0.05 M Tris buffer solution. In polystyrene containers, 0.5 g of the SiV particles were immersed in 20 ml of the Tris buffer solution and incubated at 36.5 °C for up to 24 h. After the given soaking period, the concentrations of soluble silica and calcium ions in the soaking solutions were measured by inductively coupled plasma atomic emission spectrometry (ICP-AES; Shimadzu, ICPS-7000) (n = 3).

2.3   Tracking the nucleation of vaterite in amorphous precursors

We synthesised the precursor gels of vaterite without adding Si by following the previously described carbonation method and using absolute methanol or methanol–acetone mixed solvent (methanol:acetone = 50:50 vol. ratio). The gel was aged for 12 h at room temperature. During the aging process, gel samples were collected every 10 min and analysed by attenuated total reflectance Fourier-transform infrared (ATR-FTIR) spectrometry (JASCO, FT-IR 4000 spectrometer equipped with a ZnSe prism ATR PRO 450-S attachment and liquid-nitrogen-cooled HgCdTe (MCT) infrared detectors).

3   Results and discussion

3.1   Characteristics of SiV particles consisting of oriented vaterite primary particles

When absolute methanol was used as a solvent during the carbonation process, 1.4 μm–sized spherical SiV particles with narrow size distributions were achieved (Fig. 3–1(a), denoted as SiV-100M). This morphology was consistent with the particles containing 2.6 wt% of silicon, which were prepared in methanol with a same procedure in previous report.[11] The use of a methanol–acetone mixed solvent in a volume ratio of 70:30 resulted in a slightly stretched spherical particle shape with a mean diameter of 1.7 μm and thickness of 1.1 μm (Fig. 3–1(b), denoted as SiV-70M30A). The largest deformation was observed when an equivalent volume of the mixed solvent was used, which resulted in discoidal morphologies with a mean diameter of 2.0 μm and thickness of 0.7 μm (Fig. 3–1(c), denoted as SiV-50M50A). In particular, the SiV particles tended to be increasingly flattened with increasing volume of acetone in the solvent.

Focused ion beam (FIB) sections were prepared from the most flattened SiV-50M50A particle and were observed with a high-resolution transmission electron microscope to gain an insight into the orientation and morphology of the primary vaterite particles. A stacking of layered structures with a thickness of 10–20 nm was observed in the radial sectional view (Fig. 3–2(a)). At higher magnification, a vaterite (006) lattice fringe running almost parallel to the layer was observed (Fig. 3–2(b)). Electron–beam diffraction (EBD) of the corresponding area revealed spots due to vaterite from the [110] zone axis and less intense spots from the [211] zone axis (Fig. 3–2(c)). In contrast, vaterite (020) lattice fringes running in multiple-directions were observed in the axial sectional view (Fig. 3–2(e)). EBD results showed arc-like patterns of polycrystalline vaterite from the [301] zone axes (Fig. 3–2(f)). These results clearly indicate that the primary vaterite particles were orientated with their (001) plane (c-face) towards axial axes- and with their (110) plane (ab-face) oriented towards radial axes of SiV-50M50A particle. This is unlikely to our earlier findings on primary particle structures of pure vaterite and spherical SiV particles; Vaterite consisted of 65 nm–sized spherical primary particles, which provided Debye rings with multi zone axes, while the SiV contained 5–20 nm–sized lamellae of vaterite, which provided undefined Debye rings.[11]

X-ray diffraction patterns of the SiV particles primarily showed the diffraction peaks of vaterite with a minor peak of calcite at $2\theta \approx 29°$ (Fig. 3–3). The peaks at $2\theta \approx 21°$ ((004) plane) and 25° ((110) plane) are the representative diffraction peaks from the c- and ab-faces, respectively. The peak integrated arearatios of $I_{(004)}/I_{(110)}$ (I_c/I_{ab}) were 0.17, 0.20 and 0.32 for SiV-100M, SiV-70M30A and SiV50M50A, respectively; the c/ab-face ratio was higher in SiV with a more flattened superstructure. When considering the crystalline orientation of layered primary vaterite particles in SiV-50M50A, the other SiV particles are considered to exhibit orientations similar to the primary particles. In addition, the particle spreads as its c-face expands or shrinks depending on the c/ab-face ratio; these faces stack to shape the SiV superstructures with various level of flattening. Notably, (i) all SiV particles exhibited I_c/I_{ab} ratios greater than pure vaterite (0.14) and (ii) the c/ab-face ratio increased with the volume fraction of acetone in the solvent. These trends are unique because uni-ionic planes of calcium or carbonate ions are exposed at the c-face of the hexagonal vaterite unit cell, which is known to causes high surface energy and destabilise the face.[20, 21] For SiV, the aminopropyl-functionalised silsesquioxane was expected to contribute to the enhancement of the c/ab-face ratio.

Three mass % of silicon was detected in all the SiV samples by X-ray fluorescence analysis. The fluorescent species were further confirmed by the ^{29}Si magic angle spinning-nuclear magnetic resonance spectrometry to consist of T^2 and T^3 species with mole fractions of approximately 70:30 (Fig. 4). These results indicate that all SiV particles equivalently contained a silsesquioxane that possessed non bridging oxygen (NBO)—a silanol group in most cases—at each T^2 species. In the SiV particles, the NBOs are believed to compensate the

surface energy at the *c*-face by coordinating with calcium ion planes; this coordination also probably causes he enhanced *c*/*ab*-face ratios by regulating the crystalline growth of vaterite towards the crystallites' *ab*-axis. In the same manner, the cationic species stabilize a carbonate ion plane at the *c*-face, which induced the formation of *c*-face-oriented vaterite mesocrystals with hexagonal plate morphology.[21, 22]
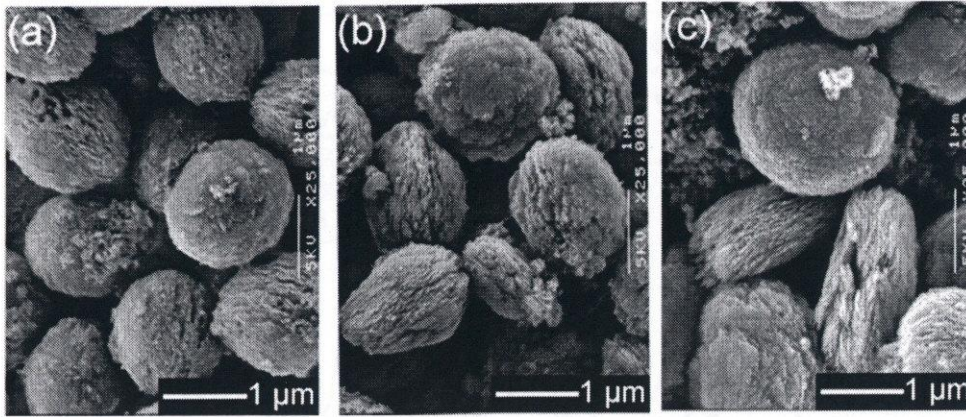
Fig. 3–1. SEM images of SiV particles. (a)SiV-100M, (b)SiV-70M30A and (c)SiV-50M50A.
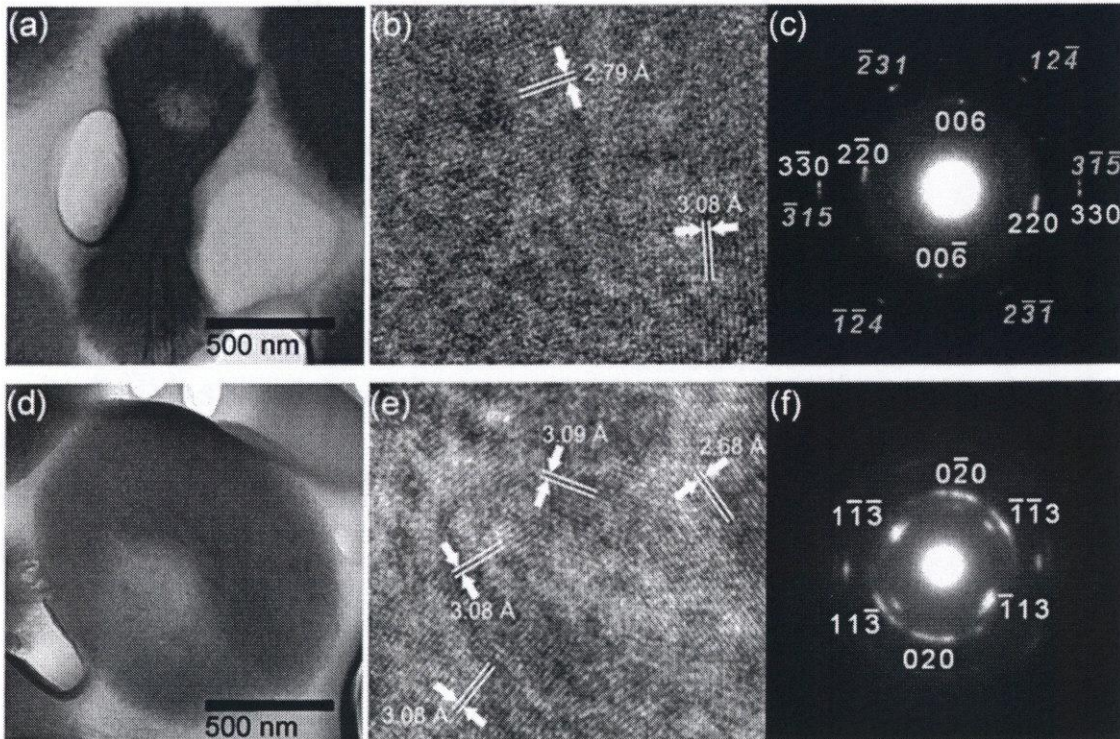
Fig. 3–2. TEM images of SiV-50M50A particle sections: (a) radial section; (d) axial section; (b, e) highly magnified images of the core parts of images (a) and (d); and (c, f) electron diffraction patterns corresponding to the areas shown in images (b) and (e).
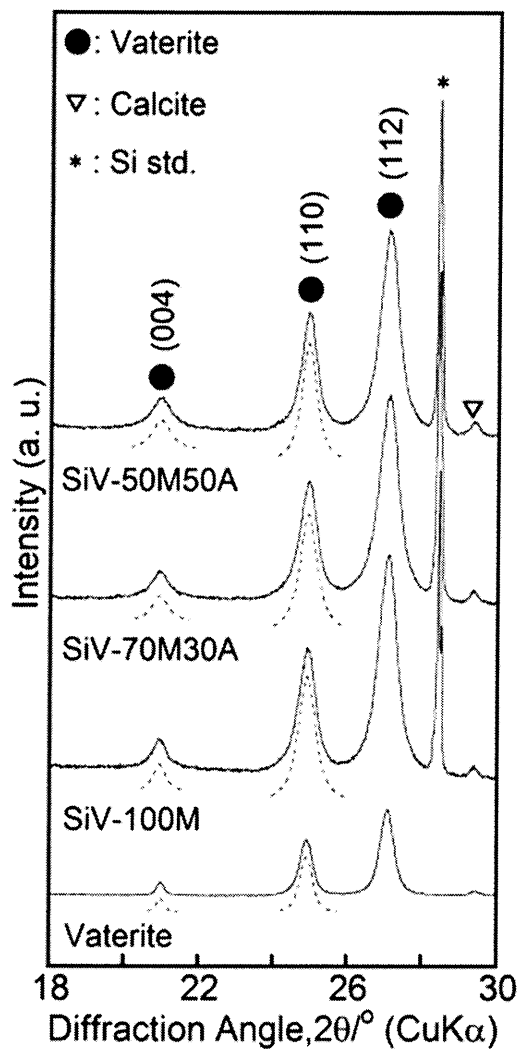
Fig. 3–3. XRD patterns of vaterite and SiV particles. The broken lines indicate the Voigt function fit of the (004) and (110) peaks.

SiV	T^2	T^3
50M50A	64	36
70M30A	63	37
100M	76	24
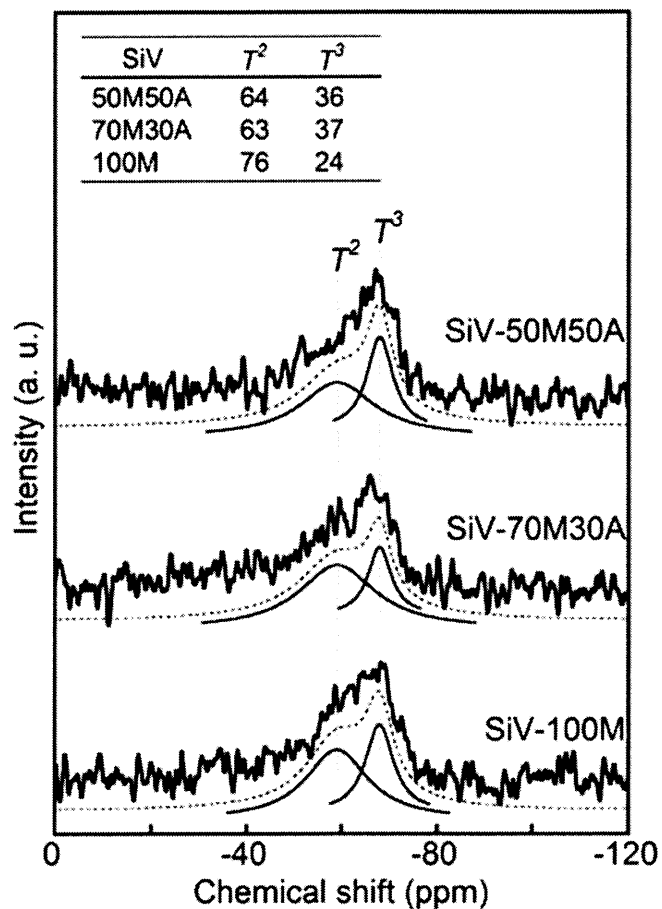
Fig. 3–4. ^{29}Si MAS-NMR spectra of SiV particles. The broken and continuous lines indicate Lorentzian function fits of the entire spectra and individual curves of T^2 and T^3 species, respectively. The inset table shows the molar fractions of T^2 and T^3 species estimated from the areas under individual curves.

3.2 Accereration of vaterite crystal growth in methanol–acetone mixed solvent

To evaluate the influence of acetone on the kinetics of vaterite crystallization, its nucleation processes from a $Ca(HCO_3)_2$ amorphous precursor gels in methanol or methanol–acetone equivalent volume mixtures were tracked by attenuated total reflection Fourier-transform infrared (ATR-FTIR) spectrometry (Fig. 3–5(a, b)). The integrated area ratio of the CO_3^{2-} peaks from vaterite and the amorphous precursor (I_v/I_a) increased exponentially with aging time (Fig. 5(c)). For an I_v/I_a ratio of 7, most of the precursor gel was converted into a white precipitate of vaterite. When the mixed solvent was used, this ratio was achieved after 60 min, which is approximately half the time required when methanol was used. Thus, the precipitation of vaterite was accelerated in the presence of acetone. Acetone has lower electrophilicity compared with methanol, which increases the supersaturation of carbonate ions and suggested to cause the acceleration.

During the formation of SiV, this reaction proceeds with the condensation of silsesquioxane in parallel.[11] The synergistic effect of oriented vaterite growth induced by NBOs in silsesquioxane, as well as the acceleration of vaterite formation by the acetone, is expected to be critical for the formation of SiV with various c/ab-face ratios (Fig. 3–6).

42
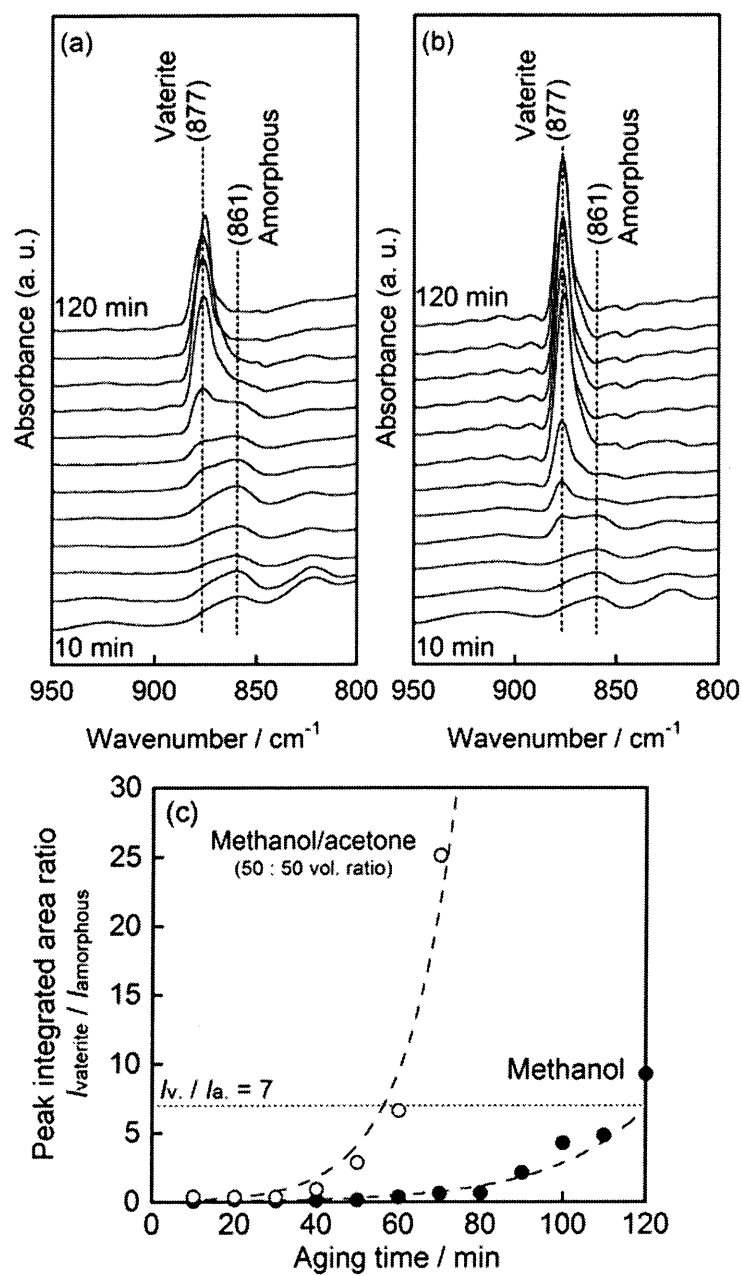
Fig. 3–5. ATR-FTIR spectra of vaterite precursor gels prepared in (a) methanol and (b) an methanol–acetone mixed solvent (50:50 vol. ratio) after the given periods of aging (at 10-min intervals). (c) Relationship between the CO_3^{2-} peak integrated area ratio in ATR-FTIR spectra and the aging time of the vaterite precursor.
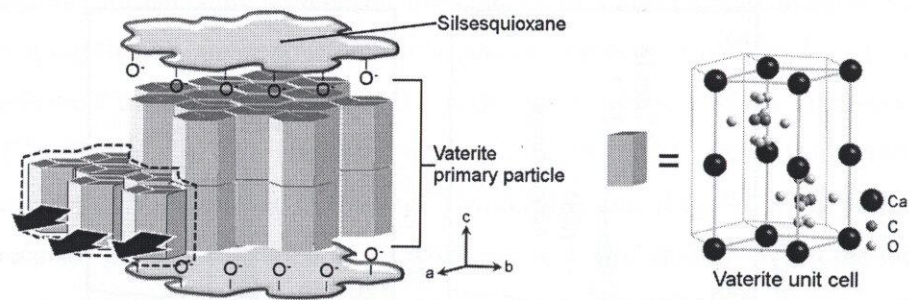
Fig. 3–6. Expected formation mechanism of primary vaterite particles with enhanced *c*/*ab*-face ratios in SiV. During the precipitation of the primary particles, NBOs of silsesquioxane coordinate to their *c*-face (calcium ion plane), which regulate the crystallization toward the *ab*-axis. The acetone in the mixed solvent increases the supersaturation of carbonate to accelerate the vaterite growth towards the *ab*-axis.

3.3 Dissolution test in Tris buffer solution

When the SiV particles were soaked in a buffer solution with pH 7.4, approximately 60 wt% of their silsesquioxane were dissolved within initial 2 h (Fig. 3–7 (a)). At the same time, the amount of Ca^{2+} ion released within 30 min decreased significantly with increasing c/ab-face ratio (Fig. 3–7(b)). In particular, the concentrations of released Ca^{2+} ions were 3.1, 2.2 and 1.6 mmol·L^{-1} for SiV-100M, SiV-70M30A and SiV50M50A, respectively. In our previous report, the vaterite in SiV was found to be enclosed in the silsesquioxane and to become soluble after most of the silsesquioxane had leached out.[11] The present result implies that primary vaterite particles were transiently stabilised in an aqueous environment by the coordination of the silsesquioxane at their c-face. This result suggests that the calcium ion release from SiV particles can be tuned by controlling their c/ab-face ratios.
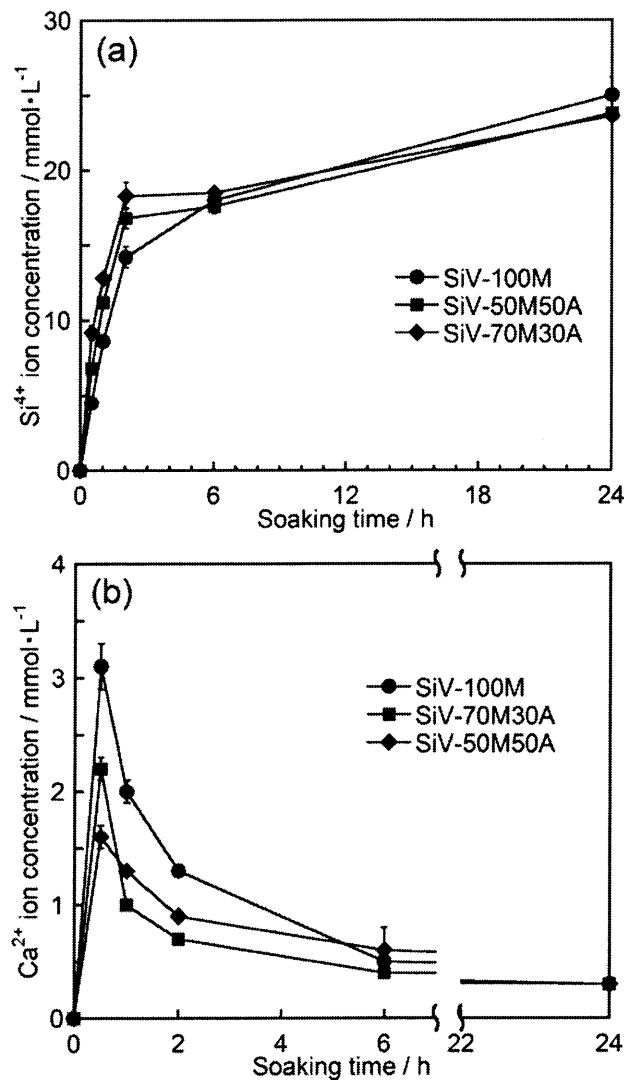
Fig. 3-7. (a) Soluble silica and (b) Ca^{2+} ion concentartion in Tris buffer solution after soaking the SiV particles for given soaking time.

4   Conclusions

- The compressed-deformation in superstructures and *c/ab*-face ratio of silsesquioxane-containing vaterite particles were controlled by changing the volume ratio of a methanol–acetone mixed solvent from 100:0 to 50:50 in a carbonation process.

- The stabilisation of the vaterite *c*-face by silsesquioxane, as well as the accelerated crystallisation of vaterite by the acetone, is proposed to be a key factor in achieving the control.

- The initial releasing amount of calcium ions from SiV could be controlled from 3.1 to 1.6 $mmol \cdot L^{-1}$ as increasing the *c/ab*-face ratio from 0.17 to 0.32, while their composition and releasing behaviors of soluble silica species were maintained.

References

[1]   T. A. Linkhart, S. Mohan and D. J. Baylink, Growth factors for bone growth and repair: IGF, TGFβ and BMP. *Bone*, **19**, S1-S12 (1996).

[2]   P. Ducy, T. Schinke and G. Karsenty, The osteoblast: A sophisticated fibroblast under central surveillance. *Science*, **289**, 1501-1504 (2000).

[3]   I. D. Xynos, M. V. J. Hukkanen, J. J. Batten, L. D. Buttery, L. L. Hench and J. M. Polak, Bioglass®45S5 stimulates osteoblast turnover and enhances bone formation; implications and applications for bone tissue engineering. *Calcif. Tissue Int.*, **67**, 321-329 (2000).

[4]   I. D. Xynos, A. J. Edgar, L. D. K. Buttery, L. L. Hench and J. M. Polak, Gene-expression profiling of human osteoblasts following treatment with the ionic products of bioglass® 45S5 dissolution. *J. Biomed. Mater. Res.*, **55**, 151-157 (2001).

[5]   J. E. Gough, J. R. Jones and L. L. Hench, Nodule formation and mineralisation of human primary osteoblasts cultured on a porous bioactive glass scaffold. *Biomaterials*, **25**, 2039-2046 (2004).

[6]   N. Patel, S. M. Best, W. Bonfield, I. R. Gibson, K. A. Hing, E. Damien and P. A. Revell, A comparative study on the in vivo behavior of hydroxyapatite and silicon substituted hydroxyapatite granules. *J. Mater. Sci. Mater. Med.*, **13**, 1199-1206 (2002).

[7]   E. S. Thian, J. Huang, M. E. Vickers, S. M. Best, Z. H. Barber and W. Bonfield, Silicon-substituted hydroxyapatite (SiHA): a novel calcium phosphate coating for biomedical applications. *J. Mater. Sci.*, **41**, 709-717 (2006).

[8]   A. Obata, T. Hotta, T. Wakita, Y. Ota and T. Kasuga, Electrospun microfiber meshes of silicon-doped vaterite/poly(lactic acid) hybrid for guided bone regeneration. *Acta Biomater.*, **6**, 1248-1257 (2010).

[9]   T. Wakita, J. Nakamura, Y. Ota, A. Obata, T. Kasuga and S. Ban, Effect of preparation route on the degradation behavior and ion releasability of siloxane-poly(lactic acid)-vaterite hybrid nonwoven fabrics for guided bone regeneration. *Dent. Mater. J.*, **30**, 232-238 (2011).

[10]   K. Fujikura, S. Lin, J. Nakamura, A. Obata and T. Kasuga, Preparation of electrospun fiber mats using siloxane-containing vaterite and biodegradable polymer hybrids for bone regeneration. *J. Biomed. Mater. Res. Part B Appl. Biomater.*, **101**, 1350-1358 (2013).

[11]   J. Nakamura, G. Poologasundarampillai, J. R. Jones and T. Kasuga, Tracking the formation of vaterite particles containing aminopropyl-functionalized silsesquioxane and their structure for bone regenerative medicine. *J. Mater. Chem. B*, **1**, 4446-4454 (2013).

[12]   T. Sugimoto, M. Kanatani, J. Kano, H. Kaji, T. Tsukamoto, T. Yamaguchi, M. Fukase and K. Chihara, Effects of high calcium concentration on the functions and interactions of

osteoblastic cells and monocytes and on the formation of osteoclast-like cells. *J. Bone Miner. Res.*, **8**, 1445-1452 (1993).

[13] S. L. Godwin and S. P. Soltoff, Extracellular calcium and platelet-derived growth factor promote receptor-mediated chemotaxis in osteoblasts through different signaling pathways. *J. Biol. Chem.*, **272**, 11307-11312 (1997).

[14] T. Yamaguchi, N. Chattopadhyay, O. Kifor, R. R. Butters, T. Sugimoto and E. M. Brown, Mouse osteoblastic cell line (MC3T3-E1) expresses extracellular calcium (Ca^{2+}_o)–sensing receptor and its agonists stimulate chemotaxis and proliferation of MC3T3-E1 cells. *J. Bone Miner. Res.*, **13**, 1530-1538 (1998).

[15] E. Eklou-Kalonji, I. Denis, M. Lieberherr and A. Pointillart, Effects of extracellular calcium on the proliferation and differentiation of porcine osteoblasts in vitro. *Cell Tissue Res.*, **292**, 163-171 (1998).

[16] O. Nakade, K. Takahashi, T. Takuma, T. Aoki and T. Kaku, Effect of extracellular calcium on the gene expression of bone morphogenetic protein-2 and -4 of normal human bone cells. *J. Bone Miner. Metab.*, **19**, 13-19 (2001).

[17] S. Maeno, Y. Niki, H. Matsumoto, H. Morioka, T. Yatabe, A. Funayama, Y. Toyama, T. Taguchi and J. Tanaka, The effect of calcium ion concentration on osteoblast viability, proliferation and differentiation in monolayer and 3D culture. *Biomaterials*, **26**, 4847-4855 (2005).

[18] U. Mayer, V. Gutmann and W. Gerger, The acceptor number — a quantitative empirical parameter for the electrophilic properties of solvents. *Monatsh. Chem. Chem. Mon.*, **106**, 1235-1257 (1975).

[19] V. Gutmann, Empirical parameters for donor and acceptor properties of solvents. *Electrochim. Acta*, **21**, 661-670 (1976).

[20] N. Gehrke, H. Cölfen, N. Pinna, M. Antonietti and N. Nassif, Superstructures of calcium carbonate crystals by oriented attachment. *Cryst. Growth Des.*, **5**, 1317-1319 (2005).

[21] A. W. Xu, M. Antonietti, H. Cölfen and Y. P. Fang, Uniform hexagonal plates of vaterite $CaCO_3$ mesocrystals formed by biomimetic mineralization. *Adv. Funct. Mater.*, **16**, 903-908 (2006).

[22] Y. Zhu, Y. Liu, Q. Ruan, Y. Zeng, J. Xiao, Z. Liu, L. Cheng, F. Xu and L. Zhang, Superstructures and mineralization of laminated vaterite mesocrystals via mesoscale transformation and self-assembly. *J. Phys. Chem. C*, **113**, 6584-6588 (2009).

Chapter IV Preparation of siloxane-containing vaterite particles with red-blood-cell-like morphologies and incorporation of calcium-salt polylactide for bone regenerative medicine

1 Introduction

Following the influential publication of Xynos *et al.*, soluble silica species have gained prominence as a promising inorganic osteogenic promoter.[1, 2] In their report, soluble silica species and calcium ions from Bioglass® 45S5 were confirmed to promote bone formation by stimulation of genes within the osteoblast cells, causing enhanced IGF-II expression.[1-3] The use of these inorganic ions as a stimulation agent for bone formation is applicable to various scaffolds fabricated with methods that involve organic solvents and heating processes.[4, 5]

Previously, the authors developed particles of vaterite-containing siloxane (SiV) for enclosure into polylactide (PLA) matrices to produce electrospun fibermats called SiPVH.[6-8] Vaterite is the least thermodynamically stable polymorph of calcium carbonate; therefore, it is soluble in body fluid and releases calcium ions. Moreover, carbonate ions are simultaneously released, which contribute to neutralise the pH decrease at the inflamed implantation site. The SiV particles also contain siloxane derived from γ-aminopropyltriethoxysilane (APTES). At the implant site, the Si–O–Si bond in siloxane hydrolyses to produce soluble silica species. Moreover, the aminopropyl moiety provides organic functional sites to bond with the carboxyl groups in PLA. The *in vitro* and *in vivo* tests were conducted on SiPVH electrospun fibermats.[6] When murine osteoblast-like cells (MC3T3-E1) were seeded, significantly larger numbers of cells were observed on the SiPVH fibermats in comparison with those on a vaterite/PLA composite. The expression of ALP was also significantly higher on the SiPVH fibermats. These results demonstrated the ability of released ions from SiV to enhance bone formation. The *in vivo* test was performed by covering a hole-shape defect (12 mmΦ) in rabbit calvarias with an SiPVH/PLA bilayer fibermat. After 4 w of culture, bone nodule was newly formed at the centre area of the fibermat, where no host bone tissue was attached.

The addition of antibiotics is commonly used in materials design with tissue engineering grafts to improve antimicrobial prophylaxis at the periphery of implant sites.[9-11] Loading antibiotic molecules on a SiV particle allows for their simultaneous release with the soluble silica species and calcium ions. The SiV particles have been prepared in methanol[6], however, in the present work, the preparation was conducted using an acetone–methanol mix solvent, which was intended for the co-addition of antibiotic molecules. PLA, a Food and Drug Administration (FDA)-approved biocompatible polymer containing a terminal carboxyl moiety that favours coordination with functional cations such as silver (I), was used in this work as a simple model molecule. The SiV particles prepared concomitantly with PLA exhibited the ability to load PLA. The structures of these

particles were characterised by electron microscopy, a nitrogen adsorption analysis, X-ray diffractometry and spectroscopic analyses. The way of PLA loading in the particles is discussed below. The dissolution tests of these particles were performed in the physiological pH buffer solution.

2 Materials and methods

2.1 Preparation of SiV particles

SiV particles were synthesised following a carbonation method in an acetone–methanol mix solvent. In summary, 10 mL of distilled water, 15 g of calcium hydroxide (Yabashi Industries Co., Ltd., Japan) and 6 mL of γ-aminopropyltriethoxysilane (Momentive Performance Materials Inc., Japan, denoted as APTES) were added to 200 mL of equivolume mixture of methanol (Wako Pure Chemicals Inc., Japan, Medical grade) and acetone (Wako Pure Chemicals Inc., Japan, Medical grade) while stirring. Each chemical was added at 20 min intervals. The slurry was bubbled with carbon dioxide gas at a rate of 2 L min^{-1} for 60 min. The gel was aged for 12 h at room temperature and then heated at 110 °C for 24 h to remove residual solvents. The resulting powder was ground to ensure the production of monodisperse particles.

PLA (LACEA$^{®}$; mass average molecular weight (M_w): ~140 kDa, polydispersity (M_w/M_n): 1.7) was heated at 250 °C for 3 h in an electrical furnace. The resulting M_w and M_w/M_n values of PLA were estimated from size-exclusion chromatography (SEC) to be 26 kDa and 1.7, respectively. This compound will hereafter be referred to as PLA_{HT}. Furthermore, the SiV particles were prepared by following the same method but with the dissolution of 5 g of PLA_{HT} in the mix solvent at the beginning of the process. Hereafter, the SiV particles prepared in the acetone–methanol mix solvent are denoted as SiV_{AM} and SiV_{AM}-PLA depending on PLA addition. The silicon content of each type of particle was estimated by dissolving a specific amount in 1 M nitric acid, and thereafter measuring the concentration of silicon with an inductively coupled plasma atomic emission spectroscope (Shimadzu, ICPS-7000; ICP-AES) (n = 3). Nitrogen adsorption–desorption isotherms were measured with a Quantachrome AS-6 Automatic Sorption Analyzer. Calcium carbonate particles containing no APTES but PLA_{HT} were also prepared by the carbonation process. These particles will hereafter be referred to as CC-PLA. The samples were evaluated with an X-ray diffractometer (PANalytical, X'pert-MPD; XRD) and an attenuated total reflectance Fourier transform infrared spectroscope (JASCO, FTIR 4000 spectrometer equipped with ATR PRO 450-S attachment; ATR-FTIR spectroscope). ^{1}H–^{29}Si cross-polarization magic angle spin nuclear magnetic resonance (^{29}Si CP/MAS-NMR) spectra of the SiV_{AM} and SiV_{AM}-PLA particles were recorded on a Varian UNITY Inova 400-plus NMR spectrometer operating at 79.49 MHz. The morphologies of the particles were observed with a scanning electron microscope (SEM) using an accelerating voltage of 15 kV (JEOL, JSM-6301F).

The dimensions of the samples were measured from obtained images using ImageJ software (US National Institutes of Health, n = 30). To image the cross-section of the SiV_{AM} particles, they were embedded in poly(methyl methacrylate) resin, and thereafter, sections were prepared by focused gallium ion beam (FIB) milling (JEOL, JEM-9320-FIB). The samples were observed with TEM at 200 kV (JEOL, JEOL-2100F).

2.2   Dissolution study in physiological pH buffer solution

Tris buffer was prepared in a water bath warmed at 36.5 °C, in which 6.118 g of tris(hydroxymethyl)aminomethane was dissolved in 900 mL of distilled water. The pH was adjusted to 7.40 using 1.0 M hydrochloric acid solution. The resulting solution was transferred to a 1 L volumetric flask and brought to volume with distilled water to achieve a 0.05 M Tris buffer solution. The dissolution study was performed by soaking 1.0 g of the SiV_{AM} or SiV_{AM}-PLA particles into 10 ml of the Tris buffer solution and incubating at 36.5 °C for 3 h. The samples were then filtered and dried at 50 °C. The dried samples were evaluated with ATR-FTIR. The concentrations of soluble silica species and calcium ions in the soaking solutions were measured with an inductively coupled plasma atomic emission spectroscope (Shimadzu, ICPS-7000; ICP-AES) (n = 3).

3   Results and discussion

3.1   Characterization of SiV particles with red-blood-cell-like morphologies

Figures 4–1 (a, c, d) show the SEM images of the SiV_{AM}, SiV_{AM}-PLA and CC-PLA particles, respectively. The SiV_{AM} particle showed a uniform specific morphology that resembled human red blood cells (Fig. 4–1(a)). The particles had a mean diameter of approximately 2 μm and a thickness of approximately 0.7 μm. From their image at higher magnification (Fig. 4–1(a) inset), the surface of the particle was found to consist of spherical particles with the diameter of 40–70 nm and their aggregates. The red-blood-cell-shaped particles were reported to form as a superstructure of planar unit particles by their multi-layered stacking.[12-14] According to the TEM observation of a SiV_{AM} particle section that was sliced perpendicular to the radial axis (Fig. 4–1(b)), the particles were found to have layers with individual thicknesses of 10–30 nm, implying that the SiV_{AM} particles consisted of planar unit structures. The morphologies with same dimensions were also observed in the SiV_{AM}-PLA particles (Fig. 4–1(c)). The CC-PLA particles were observed as a mixture of particles with two different morphologies: irregular-shaped particles with a size of approximately 1 μm and angular-shaped particles with a size smaller than 0.5 μm (Fig. 4–1(b)).

Nitrogen adsorption–desorption analysis on the SiV$_{AM}$ particles provides type IV isotherms, indicating the presence of mesoporous structures (Fig. 4–2). Their Brunauer–Emmett–Teller (BET) surface area was estimated to be approximately 76 $m^2 \cdot g^{-1}$. In addition, the adsorption–desorption hysteresis showed an intermediate shape of types H2 and H3 in IUPAC classifications.[15] In particular, type H3 hysteresis suggests the existence of slit- or wedge-shaped pores, which are formed in the aggregated planar particles. Thus, the hysteresis may correspond to the gaps between the nano-layered structures observed in Fig. 4–1(b). The SiV$_{AM}$-PLA particles exhibited a type IV isotherm with significantly narrower type H3 adsorption–desorption hysteresis compared with that of SiV$_{AM}$. A BET surface area of this sample was estimated to be 25 $m^2 \cdot g^{-1}$. These results suggested that most of the pore structures in the SiV$_{AM}$ particles were loaded with PLA molecules in the SiV$_{AM}$-PLA particles; however, certain volumes of slit-shape pores remained unloaded, which was indicated by the narrowed hysteresis shape.

The XRD patterns of these particles are shown in Fig. 4–3. The patterns from the SiV$_{AM}$ and SiV$_{AM}$-PLA particles had four diffraction peaks in the 2θ value from 20° to 35°, which corresponds to the diffractions of vaterite. The pattern from CC-PLA contained the peaks of vaterite with a notable peak at 29°, which corresponds to the main peak of calcite, the most thermodynamically stable polymorph of calcium carbonate. During the preparation of CC-PLA particles, a dissolution-reprecipitation of vaterite would occur in the solvent containing deionized water, leading to the formation of calcite, as observed in CC-PLA. In the cases of SiV$_{AM}$ and SiV$_{AM}$-PLA particles, the APTES-derived siloxane was assumed to protect vaterite primary particles from contacting with moisture and interrupt the calcite formation. Both SiV$_{AM}$-PLA and CC-PLA showed a peak at 16°, which was assigned to the diffraction peak from the crystalline part of PLA.[16, 17]

The SiV$_{AM}$ and SiV$_{AM}$-PLA particles were estimated to contain 2.0 wt% and 1.6 wt% of silicon, respectively, from the ICP-AES analysis. To achieve insight into the structure of these trace amounts of APTES-derived siloxane, ^{29}Si CP/MAS-NMR was performed on the particles (Fig. 4–4). T^n indicates the connectivity of tri-functional silane, in which T^0 indicates a single silane molecule and T^3 represents the silane connected with three Si–O–Si bridging oxygens. In the spectrum from SiV$_{AM}$, three peaks could be observed at the chemical shifts of −39 (T^0), −50 (T^1) and −59 ppm (T^2). The spectrum from SiV$_{AM}$-PLA showed peaks at −59 (T^2) and −67 ppm (T^3). These results indicate the presence of siloxane with structures as illustrated in Fig. 4. The structure with a peak at −59 ppm (T^2) may be described as a linear chain structure that terminates with T^1 species in the SiV$_{AM}$ particles. The structure with −67 ppm (T^3) contains three-dimensional branch networks in the SiV$_{AM}$-PLA particles. In addition, in these samples, siloxane consistently possesses the silanol groups of T^1 and T^2 species. Vaterite crystals are known to possess high surface energy on their c-face because of the presence of a Ca^{2+}/CO_3^{2-} uni-ionic plane. This plane is often stabilised by the supplementation of counter-charged

ionic species, which control crystal growth directions to form unique hexagonal planer vaterite particles.[18, 19] In the SiV particles, the silanol groups in the APTES-derived siloxane are presumed to play an important role in vaterite stabilization, as well as serving as a template for the formation of the planar unit particles by restricting their crystal growth in specific axis. Besides, the acetone in a preparation solvent is known to have low electrophilicity.[20] Thus, it shows the limited solubility of CO_3^{2-} ion, which also could influence the crystallization habit of vaterite. Further characterization, such as TEM-energy dispersive X-ray atom mapping and electron beam diffraction analysis would be done in the future to clarify the detailed structure of SiV_{AM} particles.

ATR-FTIR was performed on the SiV_{AM}, SiV_{AM}-PLA particles and PLA_{HT} (Fig. 4–5). In the spectrum from PLA_{HT}, the C=O stretching band from ester bonds was observed at 1749 cm^{-1}. The bands originating from the PLA backbone were observed in the area of 1000–1200 cm^{-1}, namely the C–O–C asymmetric/symmetric stretch (1182 cm^{-1}/1084 cm^{-1}), CH$_3$ rocking mode (1128 cm^{-1}) and C–CH$_3$ stretch (1044 cm^{-1}). SiV_{AM} showed a notable band at 1460 cm^{-1} and minor adsorption bands at 1128 cm^{-1} and 1030 cm^{-1}. The former is assigned to the asymmetric stretch of the CO_3^{2-} ion (v_3), and the latter is from Si–O–Si bonding from the siloxane. In the spectrum from SiV_{AM}-PLA, the bands of v_3 and Si–O–Si bonding were observed similar to SiV_{AM}. The band at approximately 1750 cm^{-1} and the increased absorption intensities in the area of 1000–1200 cm^{-1} indicated the presence of PLA molecules in the particles. Precise scans of the area from 1500 to 1900 cm^{-1} (Fig. 4–5, inset) revealed a newly formed band at 1636 cm^{-1}, which corresponds to the COO$^-$ group, suggesting the formation of a salt from the terminal carboxyl group in PLA with cations. In particular, in the SiV_{AM}-PLA particles, the source PLA_{HT} had been exposed to the calcium-rich solvent during their preparation process. We may thereby conclude that PLA predominantly formed a calcium salt (Ca-PLA) and was loaded in the mesoporous structures of the SiV particles.
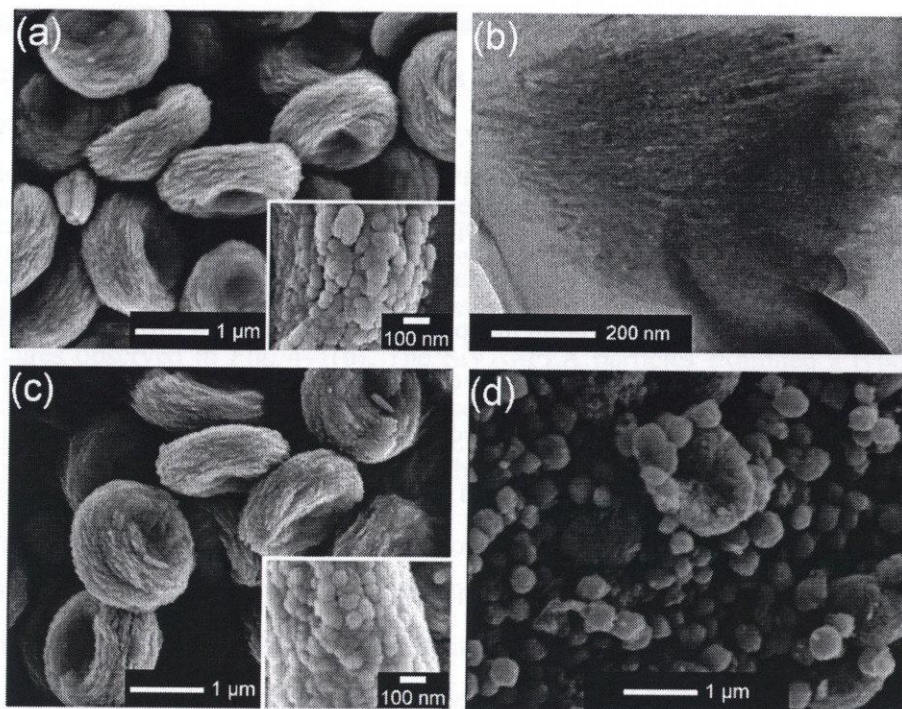
Fig. 4–1. SEM images of (a) SiV$_{AM}$, (c) SiV$_{AM}$-PLA and (d) CC-PLA particles and (b) a TEM image of FIB-sectioned SiV$_{AM}$ particle. The horizontal axis of image (b) is parallel to the radial direction of the particles.
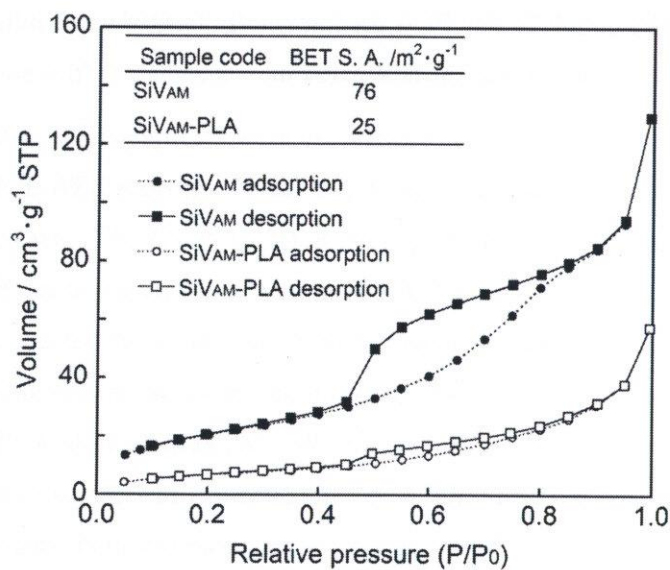
Fig. 4–2. N$_2$ adsorption–desorption isotherms of SiV$_{AM}$ and SiV$_{AM}$-PLA particles. The inset table shows the Brenauer–Emmett–Tailor surface area values of the samples estimated from the isotherms.
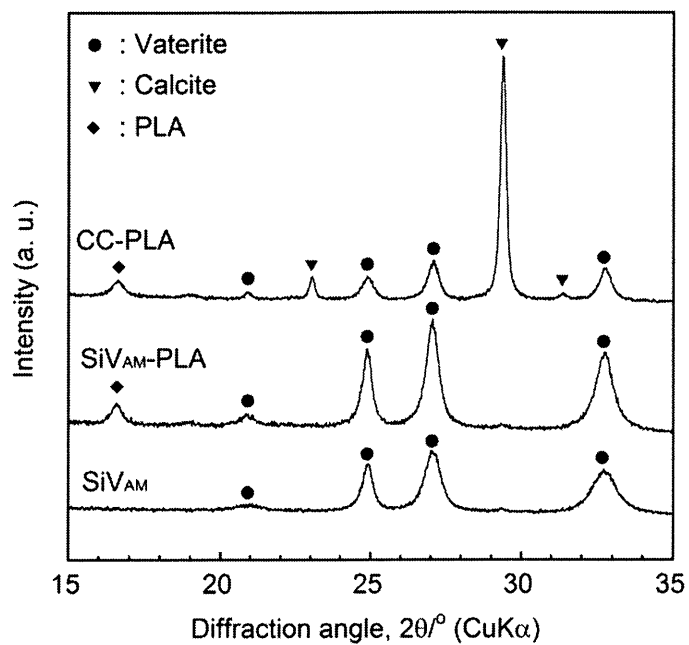
Fig. 4–3. XRD patterns of SiV$_{AM}$, SiV$_{AM}$-PLA and CC-PLA particles.
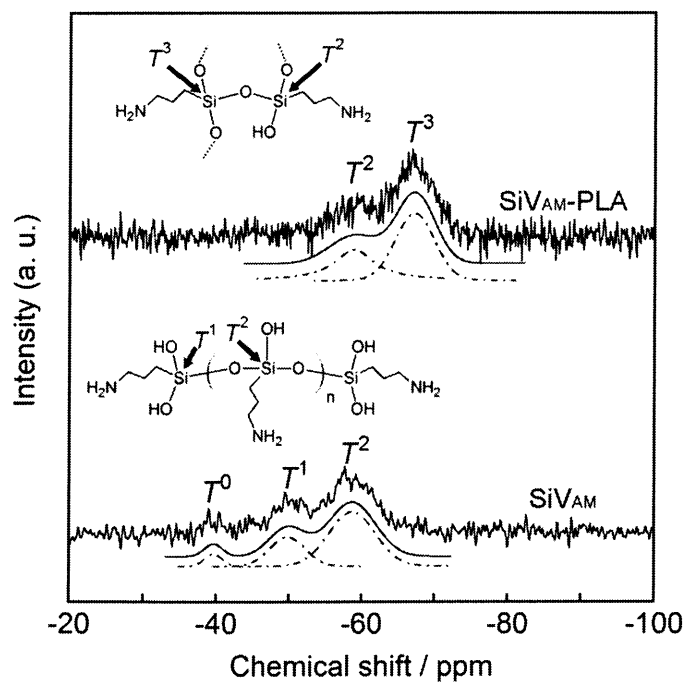
Fig. 4–4. ^{29}Si CP/MAS-NMR spectra of SiV$_{AM}$ and SiV$_{AM}$-PLA particles. The dashed lines show the Gaussian fitted peaks. The expected molecular structures of siloxane in the samples were also illustrated.
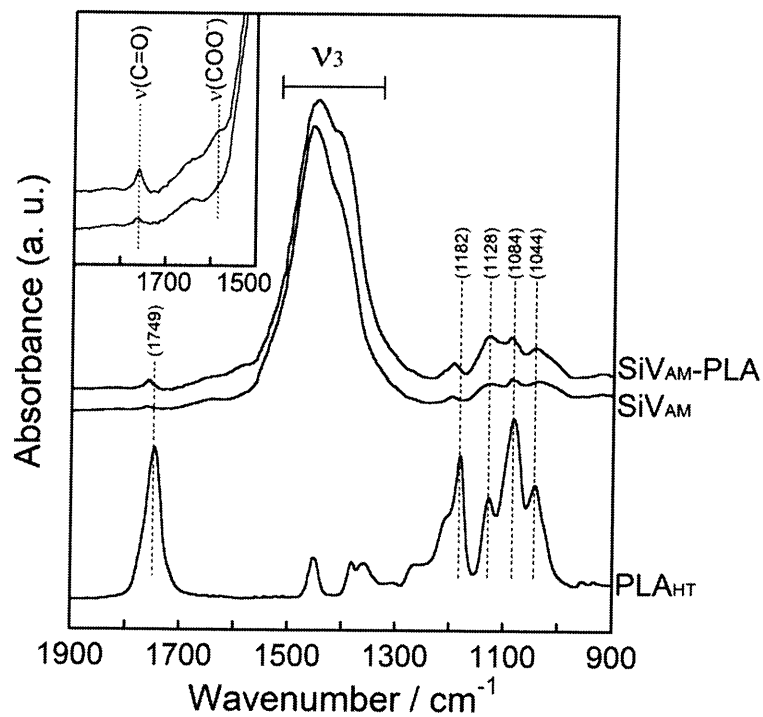
Fig. 4–5. ATR-FTIR spectra of SiV$_{AM}$, SiV$_{AM}$-PLA particles and PLA, which were used for preparation. Inset shows the intensified spectra of SiV$_{AM}$ and SiV$_{AM}$-PLA particles. Intensities of spectra from SiV samples were normalised at v_3 bands.

3.2 Dissolution behaviour of SiV particles

Short-term dissolution studies of the SiV_{AM} and SiV_{AM}-PLA particles were performed by soaking these particles in a Tris buffer solution for up to 3 h. Figure 6 shows the silicon and calcium concentrations in the solution after soaking the samples. Large increases in the concentration of silicon were observed within 1 h of soaking. During this period, fast hydrolysis of Si–O–Si bonding in aminopropyl-functional siloxane, as well as the dissolution of uncondensed APTES molecules (observed as T^0 species in the ^{29}Si CP/MAS-NMR analysis) are believed to occur, which facilitates the increase of silicon concentration. Both samples released approximately 70 mmol·L^{-1} of silicon after 1 h of soaking, an amount closely approaching the total silicon content in the SiV particles. While the release mechanisms of the silicon species were similar, calcium was released in different manner from these samples. From the SiV_{AM} particles, approximately 0.1 mmol·L^{-1} of calcium was released over the entire period of soaking. Following soaking, the particles were evaluated with ATR-FTIR (fig.4–7), which revealed that the sample showed a band at 746 cm^{-1}. This band was assigned to the in-plane bending (v_4) of CO_3^{2-} ion from crystalline vaterite, which was seen to occur even after the end of the soaking period. These results suggest that vaterite in the SiV_{AM} particles are enclosed in the APTES-derived siloxane, which physically suppresses vaterite from making contact with the soaking solution to retard calcium release. On the contrary, the SiV_{AM}-PLA particles released 1.1 mmol L^{-1} of calcium within the initial 1 h of soaking. According to the evaluation of the sample after 1 h of soaking with ATR-FTIR, a significant decrease of absorption was observed in the band of the PLA backbone vibration. Besides, an absorption band at 710 cm^{-1}, the v_4 band of calcite, newly appeared, while that of vaterite was present. The band of vaterite almost disappeared after 3 h of soaking. These results clearly indicated that the Ca-PLA molecules, which were loaded in the pore structures in the particles, as well as a part of vaterite in the particle, were released at the onset of their dissolution. This release led to the increase of calcium concentration in the initial stage of soaking.

In orthopaedic surgeries, pre- (0–2 h in advance) and peri- (~3 h afterward) surgical administration of antimicrobials is known to be the most effective method for reducing the risk of infections.[21] These dissolution behaviours suggest potential applications of SiV_{AM}-PLA as a drug vehicle in these medical applications.
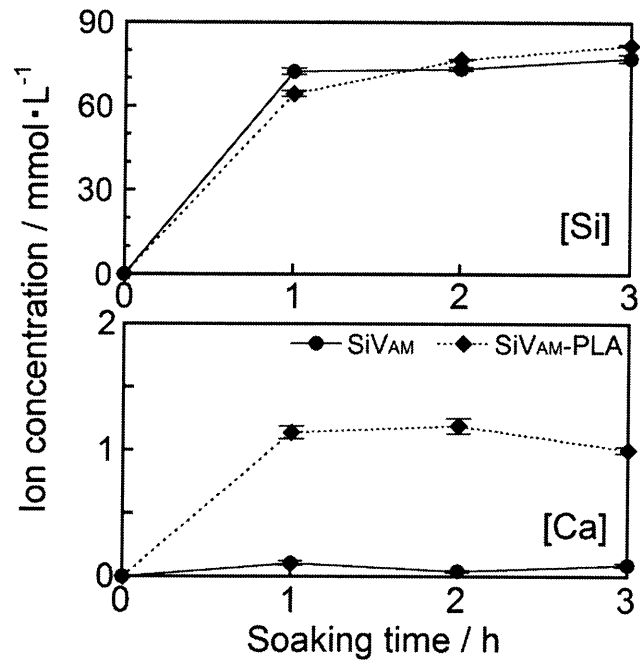
Fig. 4–6. Soluble silica species and calcium ion concentrations in Tris buffer solutions after soaking SiV_{AM} and SiV_{AM}-PLA particles for given soaking time.

4   Conclusions

- SiV particles were synthesised by a carbonation process in an acetone–methanol equivolume mix solvent (SiV_{AM}), which possessed morphologies resembling red blood cells with a mean diameter of 2 µm.
- The particles had a multilayer structure with an individual thickness of 10–30 nm, which showed characteristic hysteresis of a slit- or wedge-shaped pore in the N_2 adsorption–desorption isotherm.
- Dissolving PLA into the mix solvent prior to SiV synthesis led to the formation of a calcium salt and subsequent loading into the pore structures of the resulting SiV particles.
- In the Tris buffer solution, the SiV_{AM} particles showed fast release of soluble silica species within 1 h of soaking, whereas no significant release of calcium was observed.
- In the case of SiV_{AM} containing Ca-PLA, both soluble silica species and calcium were found to be released simultaneously within 1 h of soaking.

References

[1] I. D. Xynos, M. V. J. Hukkanen, J. J. Batten, L. D. Buttery, L. L. Hench and J. M. Polak, Bioglass®45S5 stimulates osteoblast turnover and enhances bone formation; implications and applications for bone tissue engineering. *Calcif. Tissue Int.*, **67**, 321-329 (2000).

[2] I. D. Xynos, A. J. Edgar, L. D. K. Buttery, L. L. Hench and J. M. Polak, Gene-expression profiling of human osteoblasts following treatment with the ionic products of bioglass® 45S5 dissolution. *J. Biomed. Mater. Res.*, **55**, 151-157 (2001).

[3] J. E. Gough, J. R. Jones and L. L. Hench, Nodule formation and mineralisation of human primary osteoblasts cultured on a porous bioactive glass scaffold. *Biomaterials*, **25**, 2039-2046 (2004).

[4] A. R. Boccaccini, M. Erol, W. J. Stark, D. Mohn, Z. Hong and J. F. Mano, Polymer/bioactive glass nanocomposites for biomedical applications: a review. *Composites Sci. Technol.*, **70**, 1764-1776 (2010).

[5] A. Hoppe, N. S. Güldal and A. R. Boccaccini, A review of the biological response to ionic dissolution products from bioactive glasses and glass-ceramics. *Biomaterials*, **32**, 2757-2774 (2011).

[6] A. Obata, T. Hotta, T. Wakita, Y. Ota and T. Kasuga, Electrospun microfiber meshes of silicon-doped vaterite/poly(lactic acid) hybrid for guided bone regeneration. *Acta Biomater.*, **6**, 1248-1257 (2010).

[7] T. Wakita, J. Nakamura, Y. Ota, A. Obata, T. Kasuga and S. Ban, Effect of preparation route on the degradation behavior and ion releasability of siloxane-poly(lactic acid)-vaterite hybrid nonwoven fabrics for guided bone regeneration. *Dent. Mater. J.*, **30**, 232-238 (2011).

[8] K. Fujikura, A. Obata, S. Lin, J. R. Jones, R. V. Law and T. Kasuga, Preparation of electrospun poly(lactic acid)-based hybrids containing siloxane-doped vaterite particles for bone regeneration. *J. Biomater. Sci. Polym. Ed.*, **23**, 1369-1380 (2012).

[9] R. Cancedda, P. Giannoni and M. Mastrogiacomo, A tissue engineering approach to bone repair in large animal models and in clinical practice. *Biomaterials*, **28**, 4240-4250 (2007).

[10] V. Alt, A. Bitschnau, J. Österling, A. Sewing, C. Meyer, R. Kraus, S. A. Meissner, S. Wenisch, E. Domann and R. Schnettler, The effects of combined gentamicin–hydroxyapatite coating for cementless joint prostheses on the reduction of infection rates in a rabbit infection prophylaxis model. *Biomaterials*, **27**, 4627-4634 (2006).

[11] B. J. Nablo, H. L. Prichard, R. D. Butler, B. Klitzman and M. H. Schoenfisch, Inhibition of implant-associated infections via nitric oxide release. *Biomaterials*, **26**, 6984-6990 (2005).

[12] W. Wang, Y. Hu, J. Goebl, Z. Lu, L. Zhen and Y. Yin, Shape- and size-controlled synthesis of calcium molybdate doughnut-shaped microstructures. *J. Phys. Chem. C*, **113**, 16414-16423 (2009).

[13] S. F. Chen, S. H. Yu, J. Jiang, F. Li and Y. Liu, Polymorph discrimination of $CaCO_3$ mineral in an ethanol/water solution: formation of complex vaterite superstructures and aragonite rods. *Chem. Mater.*, **18**, 115-122 (2005).

[14] M. Li, B. Lebeau and S. Mann, Synthesis of aragonite nanofilament networks by mesoscale self-assembly and transformation in reverse microemulsions. *Adv. Mater.*, **15**, 2032-2035 (2003).

[15] K. S. W. Sing, D. H. Everett, R. A. W. Haul, L. Moscou, R. A. Pierotti, J. Rouquerol and T. Siemieniewska, Reporting physisorption data for gas/solid systems with special reference to the determination of surface area and porosity (recommendations 1984). *Pure Appl. Chem.*, **57**, 603-619 (1985).

[16] F. Carrasco, P. Pagès, J. Gámez-Pérez, O. O. Santana and M. L. Maspoch, Processing of poly(lactic acid): characterization of chemical structure, thermal stability and mechanical properties. *Polym. Degradation Stab.*, **95**, 116-125 (2010).

[17] T. Kawai, N. Rahman, G. Matsuba, K. Nishida, T. Kanaya, M. Nakano, H. Okamoto, J. Kawada, A. Usuki, N. Honma, K. Nakajima and M. Matsuda, Crystallization and melting behavior of poly (l-lactic acid). *Macromolecules*, **40**, 9463-9469 (2007).

[18] A. W. Xu, M. Antonietti, H. Cölfen and Y. P. Fang, Uniform hexagonal plates of vaterite $CaCO_3$ mesocrystals formed by biomimetic mineralization. *Adv. Funct. Mater.*, **16**, 903-908 (2006).

[19] N. Gehrke, H. Cölfen, N. Pinna, M. Antonietti and N. Nassif, Superstructures of calcium carbonate crystals by oriented attachment. *Cryst. Growth Des.*, **5**, 1317-1319 (2005).

[20] U. Mayer, V. Gutmann and W. Gerger, The acceptor number — a quantitative empirical parameter for the electrophilic properties of solvents. *Monatsh. Chem. Chem. Mon.*, **106**, 1235-1257 (1975).

[21] D. C. Classen, R. S. Evans, S. L. Pestotnik, S. D. Horn, R. L. Menlove and J. P. Burke, The timing of prophylactic administration of antibiotics and the risk of surgical-wound infection. *N. Engl. J. Med.*, **326**, 281-286 (1992).

Chapter V   Preparation of Siloxane-Containing Vaterite / Poly (L-Lactic Acid) Hybrid Microbeads with Silicate and Calcium Ions-Releasing Ability

1   Introduction

Third generation biomaterials are those which are biocompatible, bioresorbable and bioactive (osteoconductive and osteoinductive).[1] Bioactive materials possess the ability to form bond to bone and some even enhance bone formation by stimulating genes in cells to proliferate and differentiate into bone cells. These properties of those materials are due to the controlled releases of silicate and calcium ions that have been reported to enhance the osteogenesis through the gene activation of the osteoblast cells.[2-4]

The injection of polymer beads suspended in biocompatible solutions has been used for maxillofacial surgeries such as augmentation of nose and chin.[5-7] This method is also ideal for achieving minimal invasive bone tissue reconstructions. An electrospraying method is an effective method for preparing the beads with a narrow distribution of diameters.[8-10] The diameter of the beads is easily controlled by adjusting the physical properties of slurry and also by varying the slurry-feeding rate. It is important to control the diameter of the beads as it effects the biological reaction of surrounding tissues such as phagocytosis or encapsulation by fibrous tissues.[11, 12]

In our earlier work, siloxane-containing polymer-inorganic (calcium carbonate–vaterite) hybrids with the releasing ability of silicate ion was prepared.[13, 14] The materials were shown to enhance proliferation and differentiation of the murine osteoblast-like cells.[15] The siloxane containing inorganic particles (SiV) derived from aminopropyltriethoxysilane (APTES) and vaterite was hybridized with poly (L-lactic acid) (PLLA) through the formation of amide bond between siloxane and PLLA through the amino groups and coordination of calcium ion in the vaterite to the carboxylic group in PLLA (these hybrids were denoted as SiPVHs).[16]

The present paper describes the preparation of bead-shaped SiPVH with ion- releasing ability for the application of minimal invasive bone reconstructions. The SiPVH beads with 10, 20 and 60 wt% of SiV particles were prepared via the electrospraying method. To evaluate their degradation behavior, the beads were soaked in a Tris buffer solution. The slurry-feeding rate and the SiV content in the slurry were varied and their effect on bead diameter and morphology was investigated. A hydroxyapatite (HA) coating layer derived via soaking in simulated body fluid (SBF) was reported to improve cytocompatibility.[13] The beads were soaked in SBF to evaluate their HA-forming ability.

2 Materials and methods

2.1 Preparation of SiV particles

SiV particles were prepared using a carbonation method described in our previous report.[17] Briefly, 150 g of $Ca(OH)_2$ and 60 ml of APTES were added into 2000 ml of methanol, stirred with blowing CO_2 gas for 75 min and the resulting slurry was then dried at 110 °C. The dried powders were spherical secondary particles of ~1 μm in diameter (specific surface area; ~70 m^2/g), consisting of vaterite with siloxane containing ~2 wt% of silicon.

2.2 Dissolution study in physiological pH buffer solution

PLLA (LACEA®; molecular weight, Mw; ~170 kDa) and SiV particles were melt-blended at 200 °C to obtain the SiPVH containing 10, 20 and 60 wt% of SiV, hereafter, these hybrids are denoted by $SiPVH_{10}$, $SiPVH_{20}$ and $SiPVH_{60}$, respectively. The beads were prepared via an electrospraying method[12]. For the investigation of SiV particle content on the bead morphology and ion-releasing ability, slurries for the electrospraying was prepared by dissolving 1.1 g of $SiPVH_{10}$, 1.3 g of $SiPVH_{20}$ and 2.5 g of $SiPVH_{60}$ containing 0.1, 0.3 and 1.5 g of SiV particles, respectively into 19.0 g of chloroform. The final PLLA to chloroform of 5 % in mass ratio was achieved for the slurries. Table 1 shows the slurries and processing conditions used to prepare the beads. In order to investigate the effect of the feeding rate on the SiPVH beads diameter, the electrospraying of the $SiPVH_{20}$ was performed by varying the feeding rate from 0.1 to 0.9 ml/min. The voltage applied to the capillary was adjusted to the minimum value at which a slurry–jet was stably formed. A glass dish filled with ethanol was used as the collector, which was stirred to avoid the aggregation of the beads.

The morphologies of the beads and their fracture faces were observed with a scanning electron microscope (SEM) (JEOL, JSM-6301F). The average diameter and standard deviation of the beads were measured from the SEM images using Image-J software (http://rsbweb.nih.gov/ij/) (n = 50). The beads were treated as they were spherical during the measurement.

2.3 Evaluation of silicate and calcium ion-releasing behaviors

50 mg of the $SiPVH_{10}$ beads prepared with the slurry-feeding rate of 0.7 ml/min and the $SiPVH_{20}$ and $SiPVH_{60}$ beads prepared with the rate of 0.5 ml/min were soaked in 10 ml of Tris buffer solution of pH 7.4 and maintained at 37 °C for 168 h. After the soaking, the beads were filtrated and dried at 50 °C for 1 d. The weight-average molecular weights (M_w) of PLLA in the beads after soaking were estimated with a gel permeation chromatograph (GPC) (Shimadzu, RID-10A), equipped with two columns (Shodex, KF-604). Si^{4+} and Ca^{2+} ion concentrations in the solutions were evaluated with an inductively coupled plasma atomic emission spectrometer (ICP-AES) (Shimadzu, ICPS-7000). Note that the amount of ionic silicon-species is measured as that of Si^{4+} ion.

2.4 Coating on the beads surface with HA

10 mg of $SiPVH_{60}$ beads prepared at a feeding rate of 0.500 ml/min were soaked in 20 ml of SBF with 1.5 times ion concentrations (1.5SBF)[18] for 24 h at 37 $^\circ$C. The sample after soaking in 1.5SBF is denoted by $HA\text{-}SiPVH_{60}$ beads, hereafter. 1.5SBF contains the following ions; 3.75 mM of Ca^{2+}, 213.0 mM of Na^+, 2.25 mM of Mg^{2+}, 7.5 mM of K^+, 223.2 mM of Cl^-, 6.3 mM of HCO_3^-, 1.5 mM of HPO_4^{2-}, and 0.75 mM of SO_4^{2-}. pH of the solution was adjusted to 7.4 by adding HCl and $(CH_2OH)_3CNH_2$. The beads after soaking were washed with distilled water, and then dried at room temperature. The surfaces of the beads after soaking were observed with an SEM. HA formation of the beads were also evaluated with an X-ray diffractometer (Philips, X'pert-MPD: XRD) and a fourier transform infrared spectrometer (JASCO, FT-IR-460 Plus: FT-IR).

3 Results and discussion

3.1 Morphologies and ion-releasing behaviors of SiPVH beads

Figure 5–1 shows the SEM images of SiPVH beads. Figure 5–1 (a–c) shows the entire shapes of SiPVH beads. The average diameters of the $SiPVH_{10}$, $SiPVH_{20}$ and $SiPVH_{60}$ beads were measured to be ~110, ~150 and ~130 μm, respectively. Depressed areas can be observed on the surface of the beads, while some of the beads have shrunk and remained spherical. During the electrospraying, on the droplet from the jet a layer of stiff shell forms due to the rapid evaporation of solvent. The inside of the beads, however, would still be wet. The beads then collect into the ethanol and the solvent inside of the beads slowly diffuse out, resulting in the depressions and the deformations. The surface irregularity of the obtained beads might be beneficial for cartilage regeneration, as often the migration of injected materials from the regeneration site is reported to be one of the main problems. Therefore these surface roughness may enable entanglement and remain in regeneration site. Figure 5–1 (d-f) shows the SEM images of the fracture face of $SiPVH_{10}$, $SiPVH_{20}$ and $SiPVH_{60}$. In the $SiPVH_{10}$ and the $SiPVH_{20}$ beads, SiV particles are embedded and enclosed by the PLLA matrix. Furthermore, the matrix formed in the $SiPVH_{10}$ beads appeared to contain smaller amount of pores than that in $SiPVH_{20}$ beads. On the other hand, in the $SiPVH_{60}$ beads the particles are in close contact and they are only partially covered with a thin PLLA film. This suggests that the mass ratio between the PLLA and the SiV particles effects the embedding of the particles in the PLLA matrix.

Figure 5–2 shows the average diameters of $SiPVH_{20}$ bead as a function of slurry-feeding rate. The diameter increased from ~65 to ~180 μm by increasing the feeding rate from 0.1 to 0.9 ml/min. The figure also shows that the size distribution of the beads widens at high feeding rates. During the electrospraying, a highly charged solution forms a conical shape (Taylor cone) at the tip of the capillary. At the apex of the Taylor cone a fine liquid jet forms, which breaks up to fine droplets.[10]

Increasing the feeding rate increases the volume of materials in the jet. This results in the formation of the large-sized droplets.

Figure 5–3 shows Si^{4+} and Ca^{2+} ions concentrations in the Tris buffer solutions after soaking the beads for given length of time. The SiV content in the beads plays an important role in the amount and rate of ions released, where the higher release is found in the samples containing larger amount of SiV. In the $SiPVH_{10}$ and $SiPVH_{20}$ beads, continuous slow releases of the ions were observed after the first 12 h of soaking. From the $SiPVH_{10}$ beads, 0.3–0.7 mg/L of Si^{4+} and 1.2–2.9 mg/L of Ca^{2+} ions were released per day, while 0.4–3.8 mg/L of Si^{4+} and 1.7–10.9 mg/L of Ca^{2+} ions were released from the $SiPVH_{20}$ beads in the same period. The $SiPVH_{60}$ exhibited rapid ion dissolution in the first 12 h of soaking. The amount of Si^{4+} and Ca^{2+} ions dissolved from the beads were measured to be 59 and 81 mg/L, respectively. After the first 12 h, the controlled dissolution of both the ions was found. The ionic silicon-species were suggested to be released as silicate ions from the beads. Figure 5–4 shows M_w of PLLA in the SiPVH beads as a function of soaking in a Tris buffer solution. The M_w values measured with GPC are believed from our preliminary experiments to include their error range within 30 kDa. Almost no change in M_w could be observed, indicating that the PLLA did not degrade in a Tris buffer solution.

In the case of conventional polymer composites having releasing ability of drugs, the releases are facilitated by their degradation. From the SiPVH beads, however, the ions were released from the materials before the onset of the M_w decrease. Thus, the ions were released independent of polymer degradation. Navarro et al. reported the formation of apatite in SBF on a PLA/calcium phosphate glass particle composite where the bioactive calcium phosphate phase was enclosed by the PLA matrix.[19] They proposed that the aqueous solutions penetrate through the polymer and reacts with the glass particles to form apatite. In the $SiPVH_{10}$ and $SiPVH_{20}$ beads, dissolution of the SiV particles probably occurs by the slow diffusion of the Tris buffer solution which penetrates through the PLLA matrix. The silicate and calcium ions released from the particle also penetrate through the matrix into the solution in a control manner, and this gave rise to the slow and continuous release of these ions. Furthermore, the particles in the $SiPVH_{10}$ beads were much more enclosed than those in the $SiPVH_{20}$ beads, which will suppress the diffusion of a Tris buffer solution, resulting in the slowest dissolution. In the $SiPVH_{60}$ beads, the SiV particles were not entirely covered by PLLA and the beads were also observed to be porous both inside and outside. Therefore they will dissolve immediately into a Tris buffer solution after the soaking. That is, the releasing behaviors of the ions are regulated by the embedding structure of the SiV particles.

Table 1. Preparation conditions of SiPVH beads.

Sample	SiV : PLLA (mass ratio)	PLLA ratio in the slurry [mass %]	Feeding rate [ml/min]	Applied voltage [kV]
SiPVH$_{10}$	10 : 90	5	0.7	17
SiPVH$_{20}$	20 : 80	5	0.1 - 0.9	19
SiPVH$_{60}$	60 : 40	5	0.5	19
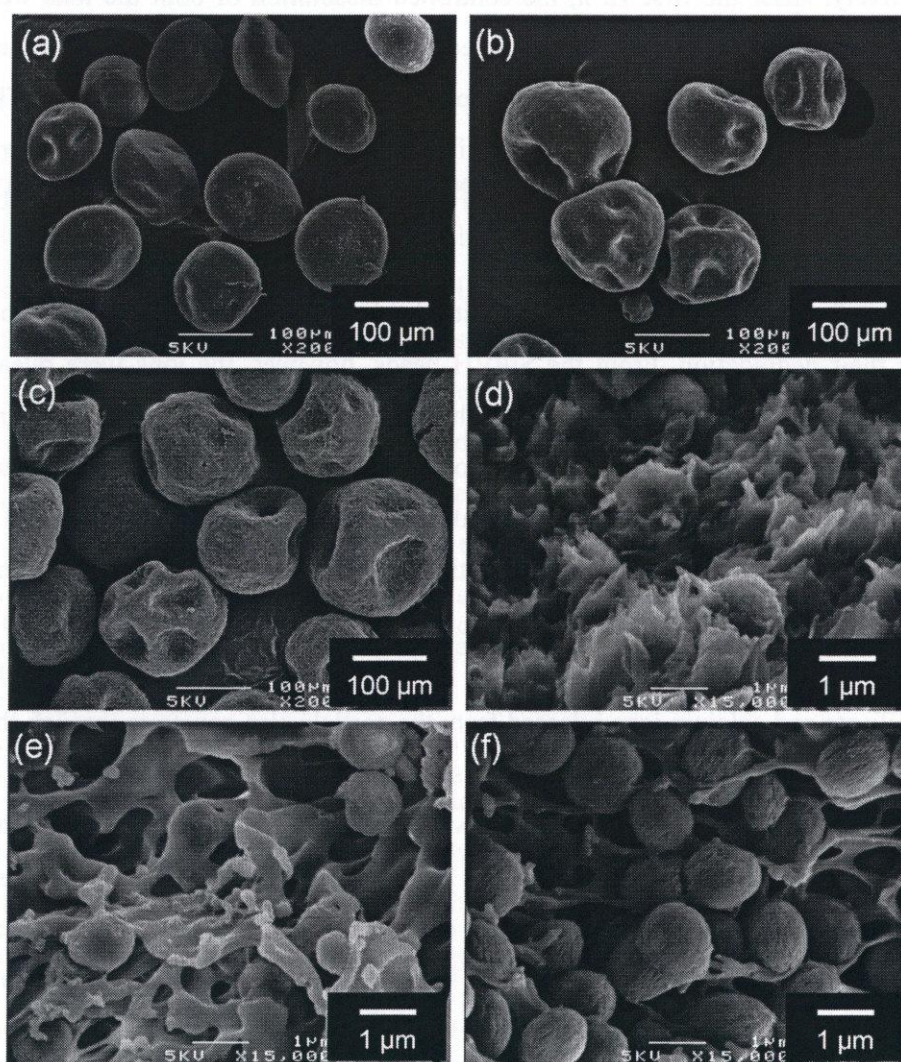
Fig. 5–1. SEM images of SiPVH beads containing (a, d) 10 wt%, (b, e) 20 wt% and (c, f) 30wt% SiV particles in PLLA matrix. (d - f) are fracture faces of (a - c), respectively.
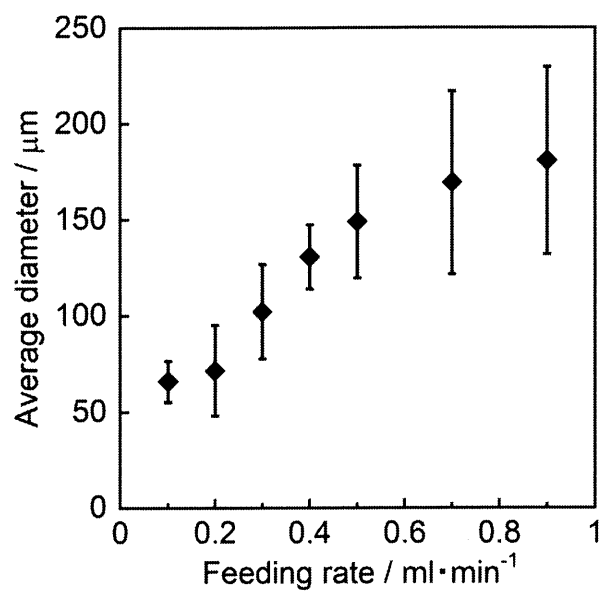
Fig. 5–2. Average diameters of SiPVH$_{20}$ bead as a function of (a) slurry-feeding rate during electrospraying and (b) SiV content in the beads.
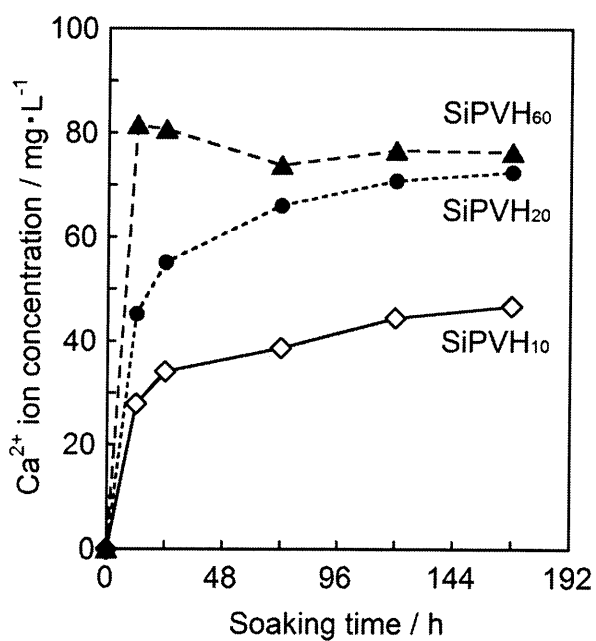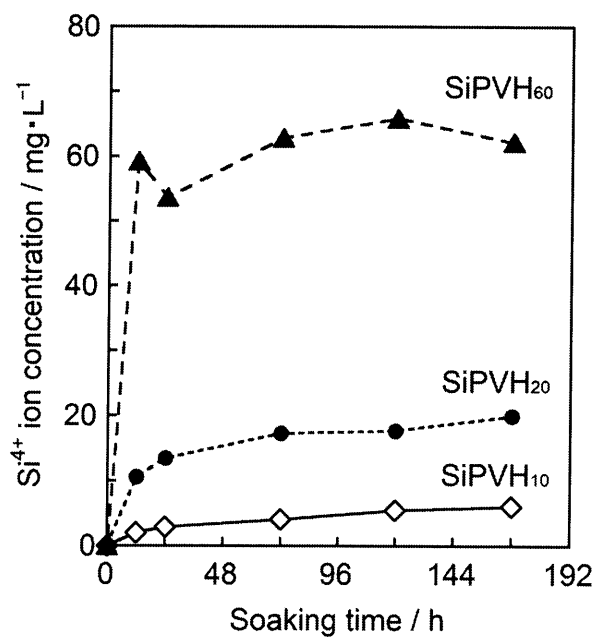
Fig. 5–3. Amount of (a) Si^{4+} and (b) Ca^{2+} ions released from the beads into a Tris buffer solution after the given period of soaking.
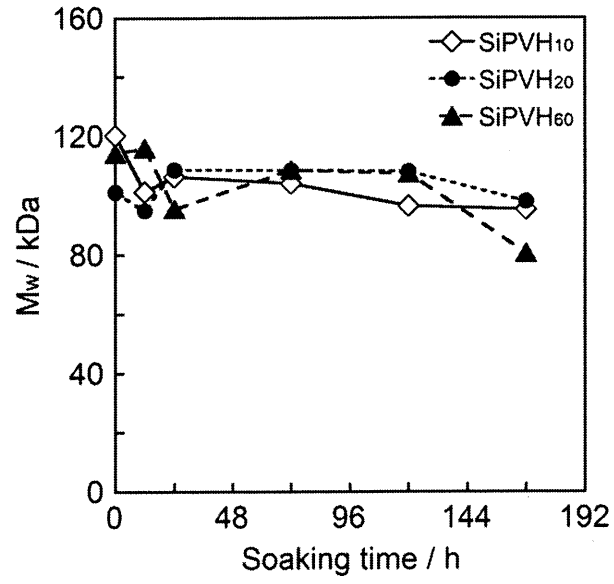
Fig. 5–4. Weight-average molecular weights (M_w) of PLLA in the SiPVH beads after soaking in Tris buffer solution.

3.2   HA formation on the surface of SiPVH beads after soaking in 1.5SBF

HA coating on the SiPVH beads is expected to be effective for improving their adhesion ability of cells. HA-forming ability of $SiPVH_{60}$ beads with diameters of ~130 μm was examined after soaking in 1.5SBF. Figure 5–5 shows the morphologies of the $SiPVH_{60}$ beads after soaking in 1.5SBF for 24 h. After the soaking, the surface of the bead was covered with leaf-shaped deposits as shown in fig. 5–5(b). Figure 5–6(a) shows the XRD spectra of $SiPVH_{60}$ beads before and after the soaking. Only one diffused peak assigned to the HA can be observed. Figure 5–6(b) shows the FT-IR spectra of $SiPVH_{60}$ beads before and after the soaking. The precipitates were successfully confirmed as HA from the double adsorption peaks at around 560 and 600 cm^{-1} assigned to the P-O bending vibration of $[PO_4]$ tetrahedral in HA.[20] HA formation on the bead surface is suggested to be induced by the carboxy group[21] in the PLLA matrix and increase of the supersaturation concerning apatite by the dissolution of the Ca^{2+} ion from the SiV particles.
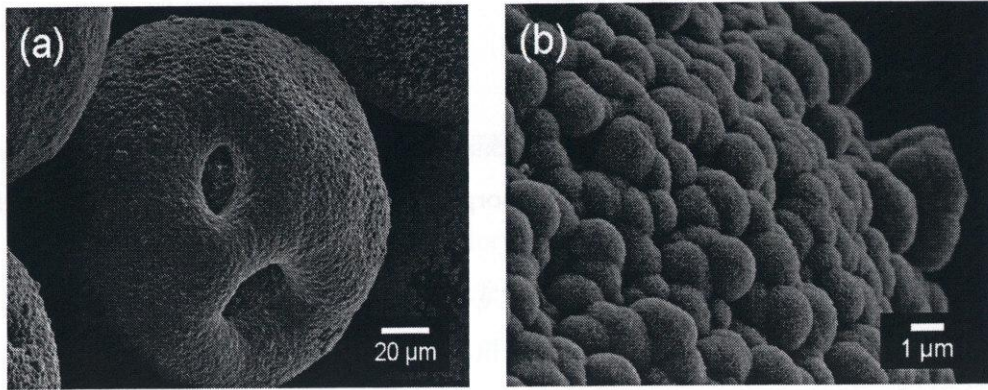
Fig. 5–5. Morphologies of SiPVH$_{60}$ beads after soaking in 1.5SBF. (a) the entire view of the beads after soaking, and (b) the highly magnified view of (a).
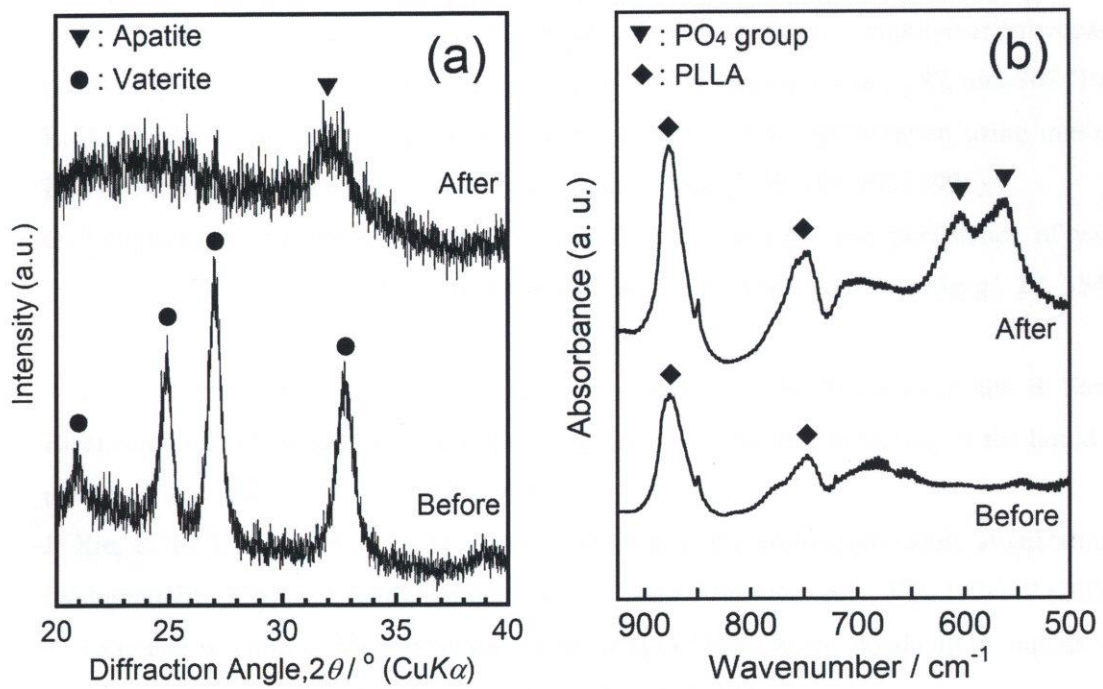
Fig. 5–6. (a) XRD spectra and (b) FT-IR spectra of SiPVH$_{60}$ beads before and after soaking in 1.5SBF.

4   Conclusions

- SiV particles were synthesised by a carbonation process in an acetone–methanol equivolume mix solvent (SiV$_{AM}$), which possessed morphologies resembling red blood cells with a mean diameter of 2 μm.

- The particles had a multilayer structure with an individual thickness of 10–30 nm, which showed characteristic hysteresis of a slit- or wedge-shaped pore in the N$_2$ adsorption–desorption isotherm.

- Dissolving PLA into the mix solvent prior to SiV synthesis led to the formation of a calcium salt and subsequent loading into the pore structures of the resulting SiV particles.

- In the Tris buffer solution, the SiV$_{AM}$ particles showed fast release of soluble silica species within 1 h of soaking, whereas no significant release of calcium was observed.

- In the case of SiV$_{AM}$ containing Ca-PLA, both soluble silica species and calcium were found to be released simultaneously within 1 h of soaking.

References

[1]   L. L. Hench and J. M. Polak, Third-generation biomedical materials. *Science*, **295**, 1014-1017 (2002).

[2]   I. D. Xynos, A. J. Edgar, L. D. K. Buttery, L. L. Hench and J. M. Polak, Ionic products of bioactive glass dissolution increase proliferation of human osteoblasts and induce insulin-like growth factor II mRNA expression and protein synthesis. *Biochem. Biophys. Res. Commun.*, **276**, 461-465 (2000).

[3]   J. R. Jones, O. Tsigkou, E. E. Coates, M. M. Stevens, J. M. Polak and L. L. Hench, Extracellular matrix formation and mineralization on a phosphate-free porous bioactive glass scaffold using primary human osteoblast (HOB) cells. *Biomaterials*, **28**, 1653-1663 (2007).

[4]   J. E. Gough, J. R. Jones and L. L. Hench, Nodule formation and mineralisation of human primary osteoblasts cultured on a porous bioactive glass scaffold. *Biomaterials*, **25**, 2039-2046 (2004).

[5]   R. A. Ersek and A. A. I. Beisang, Bioplastique: A new textured copolymer microparticle promises permanence in soft-tissue augmentation. *Plast. Reconstr. Surg.*, **87**, 693-702 (1991).

[6]   R. A. Ersek, R. B. Stovall and A. Vazquez-Salisbury, Chin augmentation using minimally invasive technique and bioplastique. *Plast. Reconstr. Surg.*, **95**, 985-992 (1995).

[7]   G. Lemperle, V. Morhenn and U. Charrier, Human histology and persistence of various injectable filler substances for soft tissue augmentation. *Aesthetic Plast. Surg.*, **27**, 354-366 (2003).

[8]   R. P. A. Hartman, D. J. Brunner, D. M. A. Camelot, J. C. M. Marijnissen and B. Scarlett, Electrohydrodynamic atomization in the cone–jet mode physical modeling of the liquid cone and jet. *J. Aerosol Sci*, **30**, 823-849 (1999).

[9]   J. Xie, L. K. Lim, Y. Phua, J. Hua and C.-H. Wang, Electrohydrodynamic atomization for biodegradable polymeric particle production. *J. Colloid Interface Sci.*, **302**, 103-112 (2006).

[10]   K. Tang and A. Gomez, Monodisperse electrosprays of low electric conductivity liquids in the cone-jet mode. *J. Colloid Interface Sci.*, **184**, 500-511 (1996).

[11]   S. Prior, B. Gander, N. Blarer, H. P. Merkle, M. a. L. Subirá, J. M. Irache and C. Gamazo, In vitro phagocytosis and monocyte-macrophage activation with poly(lactide) and poly(lactide-co-glycolide) microspheres. *Eur. J. Pharm. Sci.*, **15**, 197-207 (2002).

[12]   M. H. Mankani, S. A. Kuznetsov, B. Fowler, A. Kingman and P. Gehron Robey, In vivo bone formation by human bone marrow stromal cells: effect of carrier particle size and shape. *Biotechnol. Bioeng.*, **72**, 96-107 (2001).

[13]   H. Maeda, T. Kasuga and L. L. Hench, Preparation of poly(l-lactic acid)-polysiloxane-calcium carbonate hybrid membranes for guided bone regeneration. *Biomaterials*, **27**, 1216-1222 (2006).

[14]   H. Maeda and T. Kasuga, Control of silicon species released from poly(lactic acid)-polysiloxane hybrid membranes. *J. Biomed. Mater. Res. A*, **85A**, 742-746 (2008).

[15]   A. Obata and T. Kasuga, Cellular compatibility of bone - like apatite containing silicon species. *J. Biomed. Mater. Res. A*, **85**, 140-144 (2008).

[16]   A. Obata, S. Tokuda and T. Kasuga, Enhanced in vitro cell activity on silicon-doped vaterite/poly(lactic acid) composites. *Acta Biomater.*, **5**, 57-62 (2009).

[17]   A. Obata, T. Hotta, T. Wakita, Y. Ota and T. Kasuga, Electrospun microfiber meshes of silicon-doped vaterite/poly(lactic acid) hybrid for guided bone regeneration. *Acta Biomater.*, **6**, 1248-1257 (2010).

[18]   K. Hata, T. Kokubo, T. Nakamura and T. Yamamuro, Growth of a bonelike apatite layer on a substrate by a biomimetic process. *J. Am. Ceram. Soc.*, **78**, 1049-1053 (1995).

[19]   M. Navarro, C. Aparicio, M. Charles-Harris, M. Ginebra, E. Engel and J. Planell, in *Ordered polymeric nanostructures at surfaces*, Springer, 2006, pp. 209-231.

[20]   B. Fowler, Infrared studies of apatites. I. vibrational assignments for calcium, strontium, and barium hydroxyapatites utilizing isotopic substitution. *Inorg. Chem.*, **13**, 194-207 (1974).

[21]   T. Kokubo, H.-M. Kim and M. Kawashita, Novel bioactive materials with different mechanical properties. *Biomaterials*, **24**, 2161-2175 (2003).

Chapter VI Summary

In the present thesis, the structure and formation process of SiV particles were evaluated. Besides, a method for controlling their calcium ion release was proposed for the optimization of their ion release towards applications in bone regeneration medicine. Besides, as a future application of SiV particles in the injectable bone–fillling materials, the size-controllability, ion-release behaviour and HA formin ability of the SiPVH microbeads were evaluated.

In chapter II, SiV particles were synthesized by a carbonation process in the presence of APTES. The 5-20 nm sized vaterite lamellae in $Si_{2.6}V$ were enclosed in APTES-derived silsesquioxane and amorphous calcium carbonate. According to evaluate their precursor gel during aging stage, the condensation of the silsesquioxane and the crystallization of the vaterite were found to begin within initial an 1~2 h of aging and proceed concurrently up to 7 h of analysis period, which was suggested to favor the vaterite lamellae enclosure. In the Tris buffer solution, silsesquioxane and ACC promptly dissolved from the particles. Vaterite gradually dissolve and transformed into calcite along with the dissolution of silsesquioxane. The total dissolution times of the silsesquioxane were 6 h and 24 h for $Si_{2.6}V$ and $Si_{4.9}V$ particles, which was found to significantly influence the transformation time of vaterite. When the particles were also soaked in Mili-Q water, the T^2 species of silicon atoms were predominantly found in their leached product, which is followed by the T^1 and T^3 species. This result implied the oligomeric-aminopropylsilsesquioxane as the possible structure of soluble silica species from SiV particles.

In chapter III, the superstructure and c/ab-face ratio of silsesquioxane-containing vaterite particles were controlled by changing the volume ratio of a methanol–acetone mixed solvent in a carbonation process. The stabilisation of the vaterite c-face by silsesquioxane, as well as the accelerated crystallisation of vaterite by the acetone, is expected to be a key factor in achieving the control. The amount of calcium ions initially released from SiV decreased significantly as the c/ab-face ratio increased. These results suggested that the calcium ion release from SiV particles can be tuned by controlling their c/ab-face ratios.

In chapter IV, SiV particles were synthesised by a carbonation process in an acetone–methanol equivolume mix solvent (SiV_{AM}). The particles obtained possessed morphologies resembling red blood cells with a mean diameter of 2 μm. The particles had a multilayer structure with an individual thickness of 10–30 nm, which showed characteristic hysteresis of a slit- or wedge-shaped pore in the N_2 adsorption–desorption isotherm. Dissolving PLA into the mix solvent prior to SiV synthesis led to the formation of a calcium salt at the terminal carboxyl group and subsequent loading into the pore structures of the resulting SiV particles (SiV_{AM}-PLA). In the Tris buffer solution, the SiV_{AM} particles showed fast release of soluble silica species within 1 h of soaking, whereas no significant release of calcium was observed. In the case of SiV_{AM}-PLA, both soluble silica species and calcium were found

75

to be released simultaneously within 1 h of soaking. The calcium release was further confirmed to be facilitated by the dissolution of the Ca-salt PLA and vaterite from the particles.

Finally in chapter V, The SiPVH beads were successfully prepared by an electrospraying method and the diameter of the beads could be manipulated from 65 to 180 μm by changing the feeding rate and the SiV content in the beads. $SiPVH_{10}$ and $SiPVH_{20}$ beads showed the sustained release of silicate and Ca^{2+} ions, while $SiPVH_{60}$ showed rapid initial dissolution. This variation in ion releasing behavior originates largely from the differences in the embedding and enclosing of SiV particles in the PLLA matrix. After soaking the beads into 1.5SBF, their surface could be successfully covered with an HA layer.

Publications including studies in this thesis

1) Preparation of electrospun fiber mats using siloxane-containing vaterite and biodegradable polymer hybrids for bone regeneration

   Jin Nakamura, Akiko Obata and Toshihiro Kasuga

   Phosphorus Research Bulletin, **24**, 1-5 (2010)

2) Preparation of electrospun poly(lactic acid)-based hybrids containing siloxane-doped vaterite particles for bone regeneration

   Jin Nakamura, Gowsihan Poologasundarampillai, Akiko Obata and Toshihiro Kasuga

   Journal of the Ceramic Society of Japan, **118**, 541-544 (2010).

3) Tracking the formation of vaterite particles containing aminopropyl-functionalized silsesquioxane and their structure for bone regenerative medicine

   Jin Nakamura, Gowsihan Poologasundarampillai, Jullian R. Jones and Toshihiro Kasuga

   Journal of Materials Chemistry B, **1**, 4446-4454 (2013)

4) Preparation of siloxane-containing vaterite particles with red-blood-cell-like morphologies and incorporation of calcium-salt polylactide for bone regenerative medicine

   Jin Nakamura and Toshihiro Kasuga

   Journal of the Ceramic Society of Japan, **121**, 792-796 (2013).

5) Enhancement of crystalline plane orientation in silsesquioxane-containing vaterite particles towards tuning of calcium ion release

   Jin Nakamura and Toshihiro Kasuga

   Journal of Materials Chemistry B, Accepted December 2013. (DOI: 10.1039/C3TB21571G)

Related publications

1) Preparation of poly(lactic acid)/si-doped vaterite hybrid microbeads

   <u>Jin Nakamura</u>, Akiko Obata and Toshihiro Kasuga

   Proceedings of 22th International Symposium on Ceramics in Medicine, edited by S. Kim,

   Daegu, South Korea, 2009, pp.657-660.

2) Preparation of poly(lactic acid)/si-doped vaterite hybrid beads by electrospraying

   <u>Jin Nakamura</u>, Toshiki Hotta, Akiko Obata and Toshihiro Kasuga

   Archieves of BioCeramics Research, **9,** 131-134 (2009).

   (*Proceedings of the 9th Asian BioCeramics Symposium*)

   Nagoya, Japan, 2009

3) Effect of preparation route on the degradation behavior and ion releasability of siloxane-poly(lactic acid)-vaterite hybrid nonwoven fabrics for guided bone regeneration

   Takashi Wakita, <u>Jin Nakamura</u>, Yoshio Ota, Akiko Obata, Toshihiro Kasuga and Seiji Ban

   Dental Materials Journal, **30,** 232-238 (2011).

4) Silicate and calcium ions releasing biomaterials for bone reconstruction

   <u>Jin Nakamura</u>, Akiko Obata, Julian R. Jones and Toshihiro Kasuga

   Key Engineering Materials, **493-494,** 561-565 (2012).

5) Induction of hydroxycarbonate apatite formation on polyethylene or alumina substrates by spherical vaterite particles deposition

   Akiko Obata, Daiki Hasegawa, <u>Jin Nakamura</u>, Julian R. Jones and Toshihiro Kasuga

   Materials Science and Engineering: C, **32,** 1976–1981 (2012).

6) Mechanical-tensile strengths and cell-proliferative activities of electrospun poly(lactic-co-glycolic acid) composites containing β-tricalcium phosphate

   Shingo Ito, <u>Jin Nakamura</u>, Akiko Obata, Toshihiro Kasuga, Hitoshi Hirata

   Phosphorus Research Bulletin, **26,** 109-112 (2012).

7) Preparation of electrospun fiber mats using siloxane-containing vaterite and biodegradable polymer hybrids for bone regeneration

   Kie Fujikura, Sen Lin, <u>Jin Nakamura</u>, Akiko Obata, Toshihiro Kasuga

   Journal of Biomedical Materials Research Part B: Applied Biomaterials, **101,** 1350-1358 (2013).

Acknowledgements

At last, I would like to thank my family, especially my mother and father for always believing in me, for their continuous supports and warm encouragement for my decisions.

Jin Nakamura